Bachelor in Nanoscience and Nanotechnology

FINAL BACHELOR THESIS

MATRYOSHKA-LIKE MAGNETIC SHIELDING FOR SUPERCONDUCTING QUBITS

Olga Marco Puértolas

Supervised by Dr. Pol Forn Díaz (IFAE),

Advised by Prof. Agustí Lledós Falcó (UAB)

June 6, 2020
Department of Sciences
Autonomous University of Barcelona

INDEX

***Abstract**: "Quantum bits (qubits) are the heart of quantum computing but they are sensitive to their environment. In this thesis, the main objective is to study and apply different materials as well as geometries to find the best way to shield superconducting qubits from external magnetic fields, in particular, that of Earth. An approach to the problem is proposed and followed by simulations through the use of COMSOL Multiphysics to solve it."*

CHAPTER 1: INTRODUCTION

1.1. Background and Motivation

Quantum computing is the study of the information processing tasks that can be realized using quantum mechanical systems. [0] Classical computers store information by using bits, which can have a value of either 0 or 1. In contrast, quantum computers use **qubits** (quantum bits). A single qubit is a quantum mechanical two-level system of which one state can be either |0> ('ground' state), |1> ('excited' state) or a **superposition** of both states at the same time until it is observed. Two qubits can be entangled, meaning that their quantum state cannot be described independently of each other. The superposition of states and **entanglement** allow a more powerful and faster information platform that what is possible with classic components.

Despite the progress in the study of the superposition of two qubits states and entanglement to perform quantum computation tasks, quantum algorithms have proven to be extremely difficult to be implemented in real physical devices. In fact, the presence of **noise** and **decoherence** are the two major barriers to the implementation of quantum computing.

A general state of a qubit can be represented as a weighted sum of both states 0 and 1. Decoherence in a qubit is related to the qubit's extreme sensitivity to external **perturbations**. Due to this phenomenon, the wave function of an excited qubit undergoes random phase jumps in its value. These random quantum jumps affect to the efficiency of algorithms, such as Shor's algorithm.[0] If the coherent evolution is interrupted by a quantum jump, the computation is reported to be failed.

Due to their long coherence and potential scalability, **superconducting** qubits are used as a leading and versatile platform to build quantum computers. The operation of superconducting qubits is based on superconductivity and the Josephson effect. These systems have proved a remarkable improvement in relaxation time and scalable lithographic patterning. Using the proper choice of circuit parameters and operating conditions, superconducting qubits can be efficiently addressed for experimental control and measurement. [1]

However, in order to read out and manipulate the qubit state, the qubit needs to be coupled to the environment in a controlled way. **Cryogenic temperatures** and **ultra-high vacuum** are some of the isolation methods needed to mitigate noise from the environment affecting the qubit state, but other factors should be considered, such as external magnetic fields.

1.2. Research Goals

This final dissertation will be based on the simulation of different materials and geometries which could be used inside the cryostat, where the qubits are maintained at cryogenic temperature, in order to screen magnetic fields as best as possible. A multilayered shielding based on both high-μ and superconducting materials is studied, whose structure can remind one of that of a “matryoshka” doll, so I decided to name this project by analogy.

As for professional training goals, the opportunity to be able to realize this project meant a great chance to acquire a first-hand experience of what is like to be a part of a research group dedicated to a fascinating and promising field such as quantum computing. The aim of this project is to increase self-knowledge on this field, but also to be able to contribute, even in a small measure, in this new line of investigation. I also attempted to improve the necessary skills to become part of a research group, such as **effective communication**, **conflict management** and **teamwork** skills.

The development of this TFG was done thanks to the Quantum Computing Technology group at Institut de Física d’Altes Energies **IFAE**. It was supervised by Dr. Pol Forn-Díaz and advised by Prof. Agustí Lledós Falcó (Universitat Autònoma de Barcelona **UAB**).

1.3. Thesis Outline

Chapter 1 introduces the background, motivation and outline of this final dissertation.

Chapter 2 gives a theoretical description of relevant concepts, together with their definitions, related to magnetism as well as the materials that were studied in this research. The first part is a review of magnetism that covers a brief introduction to this field of study and the different existing magnetic materials. The second part includes a review of magnetic shielding. Superconducting and high-μ materials are introduced, including a description of properties that may be interesting for their use as magnetic shielding materials.

Chapter 3 contains the simulation carried out using finite element methods based on COMSOL Multiphysics. The modelling and simulation start from the study of the effects of an endcap using a cylindrically symmetric shield composed of high-μ or superconducting material. Different geometries were also investigated in order to obtain the best magnetic shielding for superconducting qubits. Lastly, a multi-layered shielding simulation was performed to compare investigated materials theory and simulations results.

Chapter 4 summarizes the conclusions on how to achieve the best magnetic shielding to superconducting qubits.

CHAPTER 2: LITERATURE REVIEW

2.1. Magnetic field and permeability

Magnetic effects take place when electric charges are moving. This can be in the form of an electrical current through a wire or circular currents in materials, which can be caused by electrons rotating around an atomic nucleus or around their own axes.

In order to study magnetic fields, three types of fields need to be explained: the magnetic field **H**, the magnetic induction **B** and the magnetization **M**. The magnetic field **H**, which has the unit ampere per meter (A/m), is the field applied externally to a material. The magnetic induction **B** is the number of flux lines passing through a unit area of material, whose units are tesla (T). In the vacuum, there is a directly proportion between the H-field and B-field, using the magnetic permeability of free space $\mu_0 = 4\pi 10^{-7} N/A^2$.

$$\boldsymbol{B} = \mu_0 \cdot \boldsymbol{H}. \tag{2.1}$$

If a magnetic field is applied to a certain object with magnetic properties, the magnetization **M** can be measured, **M** is defined as a measure of the magnetic moment, permanent or induced magnetic dipoles moments, per volume of material and whose units are ampere per meter (A/m).

Depending on the properties of the material, it feels a repulsive or attractive force to the applied magnetic field, which is called *magnetic behavior*, described by the relative permeability of the material μ_r. The permeability of the medium is the result of the product of the permeability of free space and the relative permeability:

$$\mu = \mu_0 \cdot \mu_r = \mu_0 \left(1 + \chi\right), \tag{2.2}$$

where χ is the magnetic susceptibility, defined as the susceptibility of a material to acquire a magnetic moment when exposed to a magnetic field $\boldsymbol{H}$. The magnetic susceptibility is the ratio of the magnetization **M** to the applied magnetic field $\boldsymbol{H}$.

When a magnetic material is present, the resulting magnetic induction $\boldsymbol{B}$ is defined as the number of lines of force passing through a unit area of material [2]:

$$\boldsymbol{B} = \mu_0(\boldsymbol{H} + \mathbf{M}) = \mu_0(1 + \chi)\boldsymbol{H} = \mu\boldsymbol{H}. \tag{2.3}$$

2.1.1. Magnetic Materials

The magnetic materials can be classified into three major types, depending on their response to an applied magnetic field and their magnetic susceptibility χ: *diamagnetic*, *paramagnetic* and *ferromagnetic*, as is shown in Figure 1. [3]

Diamagnetic materials have a negative magnetic susceptibility, usually of the order of -10^{-6} to -10^{-5}. It is negative because in an applied magnetic field, this type of material acquires an induced magnetization, which is pointed opposite to the external field. The material is repulsed by the magnetic field. The value of the susceptibility is independent of the temperature. Diamagnetic materials contain no unpaired electrons; thus, the atoms have no magnetic moment in the absence of an applied magnetic field.

All the other types of materials have positive susceptibility, meaning that the magnetization is parallel to the external field. The material is attracted to the field. The magnetic susceptibility also decreases with increasing temperature at sufficiently high temperatures, following the relationship:

$$\chi = \frac{C}{T \pm X}, \tag{2.4}$$

where C is the Curie constant and X is a magnetism type dependent constant, both being positive, independent of temperature and different for each material.

Paramagnetic materials have a small susceptibility, 10^{-4} to 10^{-5} because this type of magnetic material contain unpaired electrons on their atoms. This means that each atom has a small net magnetic moment. However, there is no interaction between each other. The efficiency an applied magnetic field in aligning the magnetic moments results in a net positive magnetization on the material. When the applied field is zero, the magnetization also becomes zero.

The magnetic susceptibility of paramagnetic materials is dependent on the temperature, following the Curie's law:

$$\chi = \frac{C}{T}. \tag{2.5}$$

Ferromagnetic materials have a critical temperature T_c, called Curie temperature, at which the variation of the magnetic susceptibility with the temperature is very different from its variation when this value is reached. *Equation 2.4* shows that, in paramagnetic materials, X increases as temperature decreases. Unlike paramagnetic materials, the spins of two neighboring electrons are oriented such that a strong interaction takes place between the atoms containing these electrons. This quantum mechanical effect explains why these atomic magnets, even in the absence of an external magnetic field, can be aligned parallel to each other.

Under the absence of an external magnetic field and below the critical temperature, the moments are aligned but when $T > T_c$, the material becomes paramagnetic, as the atoms lose their ordered magnetic moment, following the Curie-Weiss law:

$$\chi = \frac{C}{T - T_c}. \tag{2.6}$$

If the temperature decreases and approaches T_c, the magnetic susceptibility tends infinity, meaning that even when the applied field is zero, a finite magnetization can exist, known as spontaneous magnetization M_S, due to spontaneous alignment of atomic magnetic moments, which is the case of the permanent magnets. If a magnetic field is applied, the greater its strength, the more domains of the material are aligned. Eventually, the magnetization tends to a constant value, called the saturation magnetization. [4]

The typical temperature dependence of the magnetic susceptibility for ferromagnetic and paramagnetic materials is represented in Figure 2.

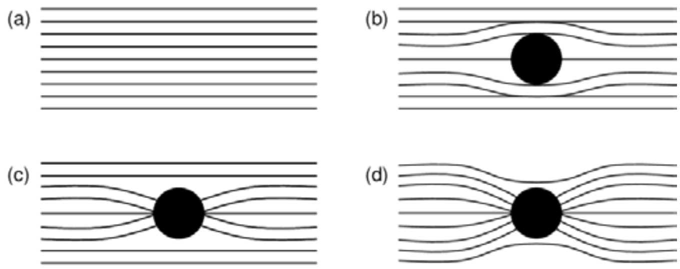

Figure 1. *The effect of magnetic materials on an (a) uniform magnetic field. (b) Diamagnetic. (c) Paramagnetic. (d) Ferromagnetic.* [1]

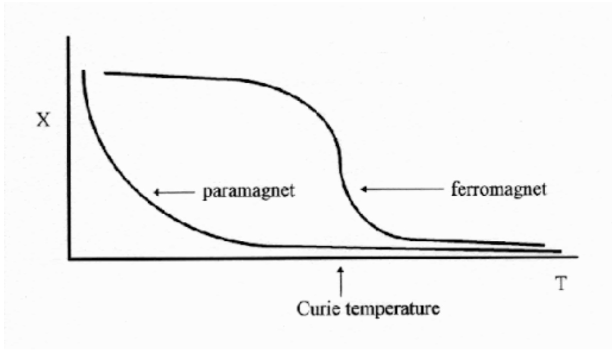

Figure 2. *Magnetic Susceptibility vs Temperature of Paramagnetic and Ferromagnetic materials.* [2]

2.2. Magnetic shielding

Magnetic shielding is a process of limiting magnetic flux in a space. This can be achieved either by passive or active shielding. Active shielding is based on the generation of fields of the same value that the external one but at opposite polarization to cancel the incident fields in the desired shielded region. Passive shielding is based on the use of magnetic shielding materials. The latter is the most convenient to use, because of the ease of implementation, as it requires no action and no energy consumption.

In this project, we define the shielding efficiency or shielding factor to describe the magnetic shielding capability of a material as:

$$\mathrm{SF} = \frac{H_0}{H}, \tag{2.7}$$

where H_0 is the magnetic field strength at a point before introducing the shield, and H is the magnetic field strength at the same point inside the shield due to H_0.

Magnetic shielding is necessary in the case of devices that cannot operate in the presence of a magnetic field or where its measurements can be interfered by the presence of an uncontrolled, fluctuating field.

2.2.1. High permeability materials

Materials used for magnetic shielding are usually selected by their **permeability** and **saturation**. Permeability is related to the effectiveness with which a given material can entrap the magnetic flux by offering it a low reluctance path. The magnetic reluctance represents the opposition to magnetic flux. Saturation is related to the maximum flux density that a given shield can capture. This depends on its thickness and the intensity of the applied magnetic field. Permeability and saturation are inversely related.

As seen in section "2.1.1", ferromagnetism is the phenomenon of spontaneous magnetization -the magnetization exists in the material even in the absence of an applied magnetic field. The best-known examples of ferromagnetic materials are the transition metals Fe, Co and Ni.

The presence of a sufficiently strong magnetic field H causes the alignment of the high-μ material dipoles in the direction of the field. The material remains magnetized even when the magnetic field is turned off, called remanence. This phenomenon can be visualized in Figure 3.

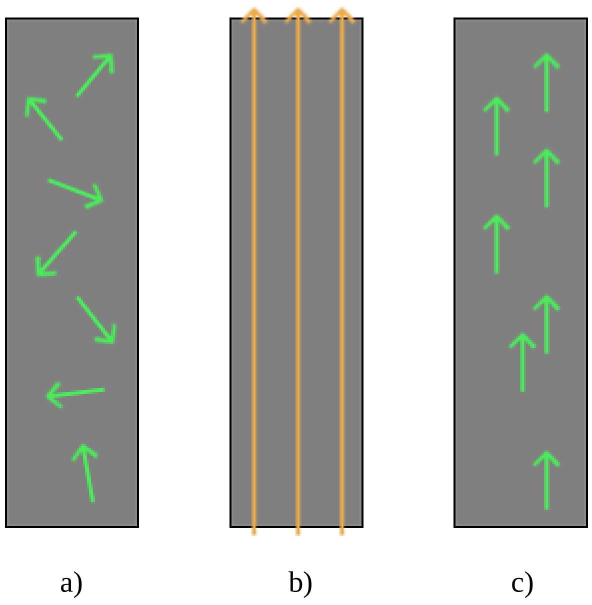

Figure 3*. Magnetization of a high-μ material. Green: small dipoles, Orange: Applied magnetic field*
a) Zero magnetization $H = 0$ b) $H \neq 0$ c) Magnetization by remanence.

Because of the remanence, there is a hysteresis relation between the magnetization M inside the material and the external applied field H, as shown in Figure 4. Once the saturation magnetization is reached, the original initial state is rarely obtained again.

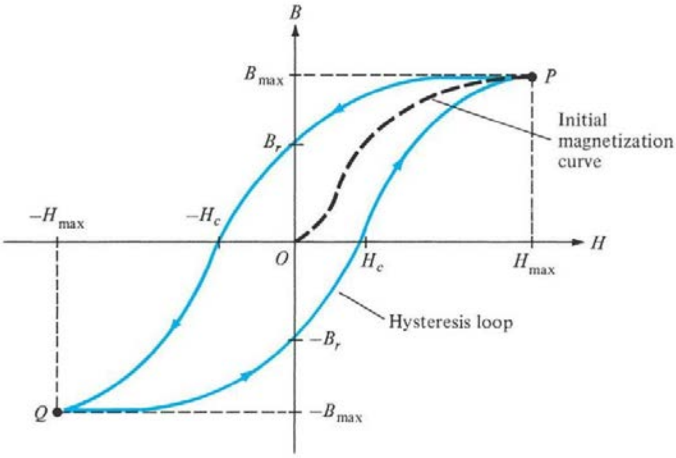

***Figure 4**. Hysteresis loop for a high-μ material.* [3]

Another of the consequences of a high permeability is the absence of magnetic induction parallel to the surface. In fact, the higher the permeability, the lower the parallel component close to the surface. So, using a material with a high-μ, $B_{II} = 0$ just outside the surface.

Amumetal[5], A4K[5] and Cryoperm[6] are some of the Ni-based ferromagnetic super alloys (permalloys) commonly used as passive shielding material. Though originally μ-metals are used for room temperature applications, there is a growing interest in using them at cryogenic temperatures. However, at low temperatures the permeability of most high-μ materials drastically drops. As a solution, some companies developed μ-metals that instead of decreasing, its permeability increases at low temperatures, such as Cryophy. [7]

2.2.2. Superconducting materials

Superconductivity was discovered by Heike Kamerling-Onnes at the Leiden Laboratory in 1911. [9] He was studying the resistance of solid mercury at cryogenic temperatures using liquid helium as a refrigerant, and at 4.2K and 1 atm he realized that its resistance was suddenly zero. The temperature at which the resistance of a superconductor drops to zero, maintaining this value below such temperature, is called the transition or **critical temperature** T_c (Figure 5). [9] The superconductors of type I were the first ones to be discovered, such as Tl, In, Sn, Hg, etc. These superconductors allow no magnetic flux through them. Type II superconductors, which do let magnetic flux through them, will not be studied in this project.

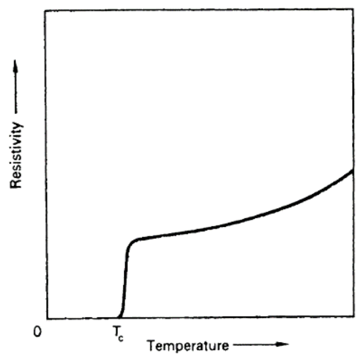

***Figure 5.** Resistivity vs Temperature for a superconducting material.*

The Meissner effect was discovered 22 years after the discovery of superconductivity by Walther Meissner and Robert Ochsenfeld[9]. The Meissner effect explains that a metal in a superconducting state never allows the existence of magnetic flux density in its interior.

$$\boldsymbol{B} = \mu_0(\boldsymbol{H} + \mathbf{M}) = 0 \rightarrow \boldsymbol{H} = -\boldsymbol{M}. \tag{2.8}$$

Therefore, the susceptibility becomes:

$$\chi = \frac{dM}{dH} = -1. \tag{2.9}$$

In fact, the Meissner state can be explained as super-currents running over the materials surface, cancelling the applied magnetic field $\boldsymbol{H}$.

Ideally, surface currents can exist only when an external magnetic field is applied to a superconductor. If the external field is switched off, the surface current ceases to occur. However, the presence of holes in the material can lead to remanent trapped flux.

Magnetic field lines outside a superconductor are always tangential to its surface. As we know from electrodynamics, the lines of the magnetic induction $\boldsymbol{B}$ are continuous and closed. The components of $\boldsymbol{B}$ normal to the surface must be equal inside and outside the material. Indeed, as in the interior of a superconductor $B_n^i = 0$, consequently, the normal component outside of the superconductor's surface is zero too: $B_n^e = 0$.

Consequently, a superconductor in an external magnetic field always carries a supercurrent near its surface (Figure 6). Only surface currents are possible, there are none in the interior of the superconductor. The surface current j_s is completely dependent on the magnetic field $\boldsymbol{H}$ at the surface. The surface current generates a magnetic field that has the same magnitude as the external magnetic field, but in opposite direction. This results in an interior field magnitude of $\boldsymbol{B} = 0$.

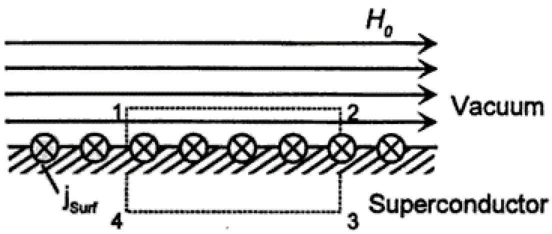

Figure 6. *Superconductor placed in a magnetic field.* [4]

Zero electrical resistance below a critical temperature and the **Meissner state** are the two key properties of superconducting materials relevant for **magnetic shields**.

However, in reality, the magnetic field does penetrate the superconducting material a certain depth. The **penetration depth $\boldsymbol{\lambda}$** is a material- and temperature-dependent parameter. In fact, there would be the same amount of flux inside the material if the flux density of the external field remains constant to a distance λ into the metal:

$$\int_0^\infty B(x)dx = \lambda B(0). \tag{2.10}$$

London's theory [10] predicts that a specimen much thicker than the penetration depth will show an exponential decay as it penetrates, as shown in Figure 7.

$$\boldsymbol{B}(x) = \boldsymbol{B}(0)e^{-\frac{x}{\lambda}}. \tag{2.11}$$

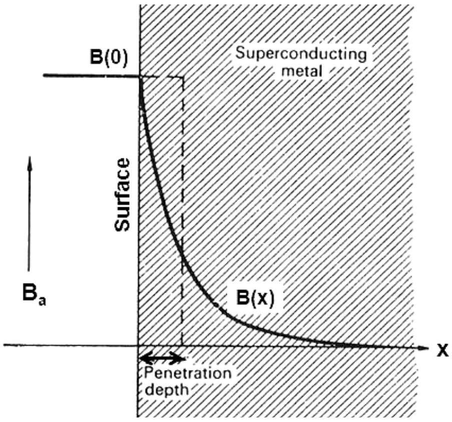

Figure 7. *Exponential decrease of the magnetic flux B with the distance x into a bulk superconductor.* [5]

The London's theory is a mathematical way to explain the Meissner effect. In fact, the phenomenon of the Meissner state is described by the equation (2.11): when a superconductor is placed in an external static magnetic field, spontaneous supercurrents appear on the surface of the material up to a penetration depth λ, creating an opposing field, which exactly cancels the field inside. [11]

The Meissner effect will break down when the external field increases beyond a certain value. Type I superconductors return to a normal state. The magnetic flux simultaneously penetrates the entire sample. The magnetization of the sample drops to zero, thus the value of the internal magnetic field becomes equal to the external field.

The Meissner effect differs from the behavior of a perfect conductor $(\sigma = \infty)$. If an external magnetic field is applied after lowering the temperature, both a perfect conductor and a superconductor can expel the magnetic field from the inside. However, if the sample is cooled after applying the magnetic field, for a superconductor the magnetic field is still expelled from the inner geometry (after the sample is cooled below its T_c), whereas for an ideal conductor, the magnetic field remains within the geometry, as shown in Figure 8. The magnetic expulsion in a perfect conductor is caused by Lenz's law. [11]

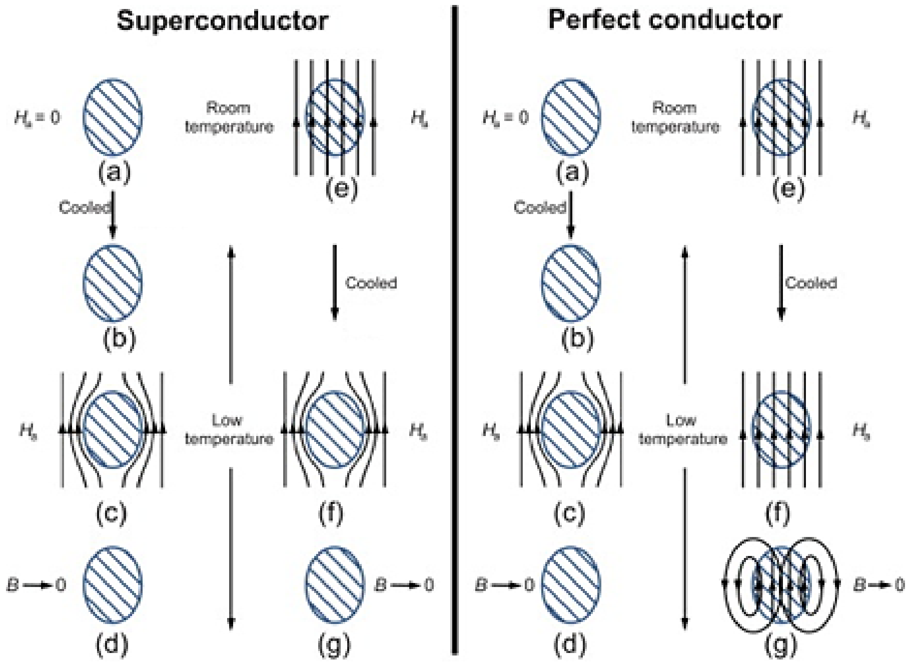

Figure 8. *Magnetic behavior of a superconductor and perfect conductor material* [6]*:* *<u>Case I (a)-(d): the magnetic field is applied after cooling</u>: (a)-(b) In the absence of a magnetic field, both materials have zero resistance; (c) Magnetic field is applied to the material;(d) The magnetic field is removed and* $\boldsymbol{B} = 0$.

<u>Case II (e-g) the magnetic field is applied before cooling</u>: (e-f) The superconductor, after cooled below its T_c*, has zero resistance. In the perfect conductor, the magnetic field remains inside. (g) Applied magnetic field is removed. The superconductor shows* $\boldsymbol{B} = 0$ *but the magnetic field remains in the perfect conductor.*

Practical applications of superconductivity are improving every year. However, the use of superconducting devices is limited by different reasons, such as the need to prevent thermal excitation. For example, this type of material is used to build **transmon qubits**[12], whose essential elements are **Josephson junctions**. This device consists of two superconducting electrodes separated by a week insulating barrier.[12]

However, the main problem of using a superconductor as a magnetic shield is the **remanent magnetization**. This effect can be produced by geometric flux trapping and vortex trapping. [11] The latter is caused on superconductors type II, so it will not be explained.

Remanent magnetization caused by the geometry of the superconductor can be produced if a magnetic field is present during the cool down through the critical temperature T_c. This magnetization is caused because of the presence of imperfections, such as holes.[11] After turning off the applied magnetic field, the interior field may not show a magnitude of $\boldsymbol{B} = 0$.

However, the remanent trapped flux can be prevented by adding a high-μ metal shield. The remanence would be minimised by making sure that only a low magnetic field is present during the cooling down. This situation will be discussed in the following chapter (Ch.3).

The remanent effect is also observed in high-μ metal, as seen in the previous section (Sec “2.2.1.”).

CHAPTER 3: EXPERIMENT AND SIMULATIONS

3.1. “FEM” modeling using COMSOL Multiphysics

In this thesis, COMSOL Multiphysics[13], a finite element modeling (FEM) is used. Specific modules can be accessed to solve and simulate different kinds of physics and engineering problems. In order to estimate the influence of magnetic fields in COMSOL, the “Magnetic Fields, no Current” in the AC/DC Module was used, as is detailed in “Annex A”.

COMSOL Multiphysics[13]is a finite-element solver, meaning that before performing its calculations, the analysed geometry is separated in different elements, forming a mesh. The outcomes of the simulation depend on the maximum size of the geometry of the mesh elements. In this project, the mesh selected is formed by several tetrahedrons of different size. The solution is constructed element by element of the mesh. [14] This result in an approximate solution based on the imposed boundary conditions and solving a set of differential equations.

In addition to the geomagnetic field, superconducting qubits can be affected by several magnetic fields from within the laboratory (such as cable conduits, furniture, structural beams, etc.), whose value could be comparable to the one of the Earth, or even higher. In this project, the value of the external magnetic field used was $B = 5 \cdot 10^{-5}\ (T)$. The magnetic shielding was evaluated by calculating both transverse and axial magnetic field components in a cylindrical geometry.

Several different arrangements of superconducting and high-μ materials for magnetic shielding were examined. A superconductor in the Meissner state displays $\mu_r = 0$. As this value cannot be applied in the software, a study to obtain the best approximation was made, as recommended by the Superconductivity Group (UAB). In the simulation this was approximated by using $\mu_r = 10^{-6}$. [15][16]

The shielding effectiveness (2.7) of a shield depends on its shape, size, thickness, number of layers and permeability of the material used. Possible problems such as the presence of holes in the shields could provide a path for the magnetic field to enter the space to be shielded and decrease the shielding factor. This problem was also studied and presented in the “3.3. Superconducting materials” section.

3.2. High-μ materials

Mumetal[17]and Cryophy[18]are the high-μ materials studied in this project.

These materials have a high content of Ni-based ferromagnetic superalloys and have high permeability values, about 80000 to 100000 than the normal steel alloy. High-μ materials are ideal materials to be used in cryogenic temperatures as passive magnetic shields. However, the permeability of these materials can change with temperature, applied magnetic field, defects in the material, application of stress or residual stresses. In fact, Mumetal permeability can be affected by cryogenic temperatures, while the Cryophy one increases by lowering the temperature. Their characteristics will be discussed in the following “3.2.1. Mumetal simulation” and “3.2.2. Cryophy simulation” subsections.

3.2.1. Mumetal simulation

Mumetal[17] is primarily composed of 80-82% Nickel and 3.5-6% Molybdenum but also contains varying quantities of Silicon, Manganese and Carbon, and balance Iron[17] [19].This alloy has a permeability of typically 80000 at 40 Gauss and up to 350000 at several thousand Gauss[19].In this project, the magnetic fields to be shielded have a value of less than 1 Gauss, so the permeability used was $\mu_r = 80000$.

As seen in the “2.1.1. Magnetic Materials” section, magnetic shielding made with high-μ materials work not by eliminating or cancelling magnetic fields, but by providing a low reluctance path for the magnetic flux around the shielded area.

High permeability Ni-Fe alloys have equivalent magnetic features. However, Mumetal shows more ductile features and provides good performance to be easily forged in the thin sheets that are normally used for magnetic shielding.[19]

Mumetal was designed to be used as the “warm” magnetic shield outside the fridge of the qubit refrigerator, as shown in Figure 9.

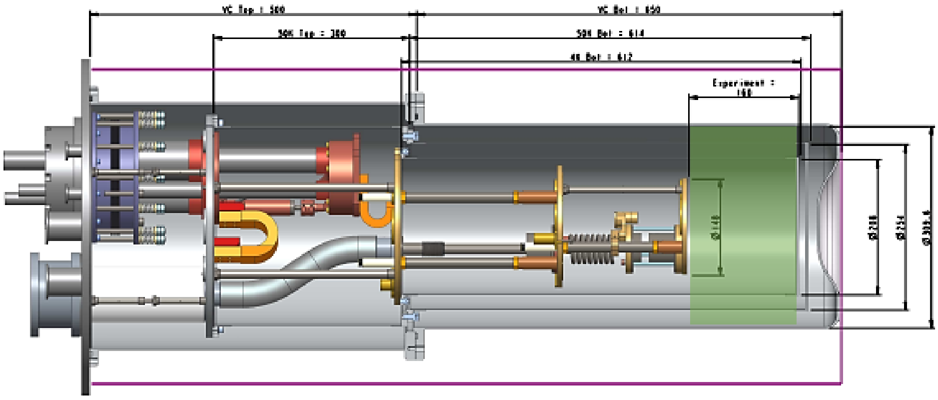

Figure 9. *Purple: Mumetal shield placed at cryostat from the Quantum Computing Technology group. Green: Experiment Area*

3.2.1.1. Open or end cup cylinder

Hollow spheres provide the best shielding properties, but they are very difficult to make and highly impractical. Based on the shape of cryostats, the most commonly used geometry for magnetic shields is cylindrical. [20]

A spherical shield is preferable by thinking of the equal shielding efficiency in all directions. In contrast, the direction of the applied field affects to the cylinder shielding efficiency. However, the axial shielding efficiency of axial cylindrical shields can be improved by using end caps. A simplified explanation is that shielding caps “attract” an extra magnetic flux that leaks inside the shield from below. [21]

However, the addition of end caps significantly reduces the magnetic field at the ends of the cylinder, but not near the central axis of the shield. [22] End caps effectively keep magnetic flux in the axial direction from entering the ends of the shield. The length of the shielded region extends towards the ends of the cylinder. Even so, the axial shielding factor can be reduced as end caps could redirect flux towards the axis and away from the cylinder walls. [23] End caps are expected to have a little, if any, effect on the transverse shielding factor.

The shielding effectiveness was used to characterize the magnetic shielding[24]:

$$\text{S.E.} = -20\log\left(\frac{H}{H_0}\right). \tag{3.1}$$

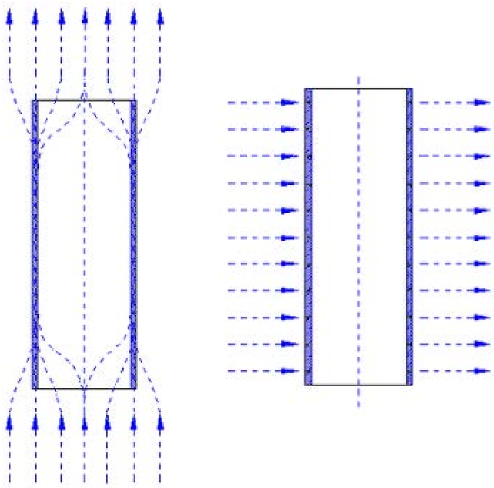

Figure 10. *Open high-μ cylinder reaction to axial (left) and transversal (right) magnetic field.*

The first simulations were an made for an open and end cap cylinders with length L = 1150mm, diameter D = 465mm and thickness t = 1mm. However, in order to speed up the simulation, the parameters were proportionally reduced by half (Figure 11)

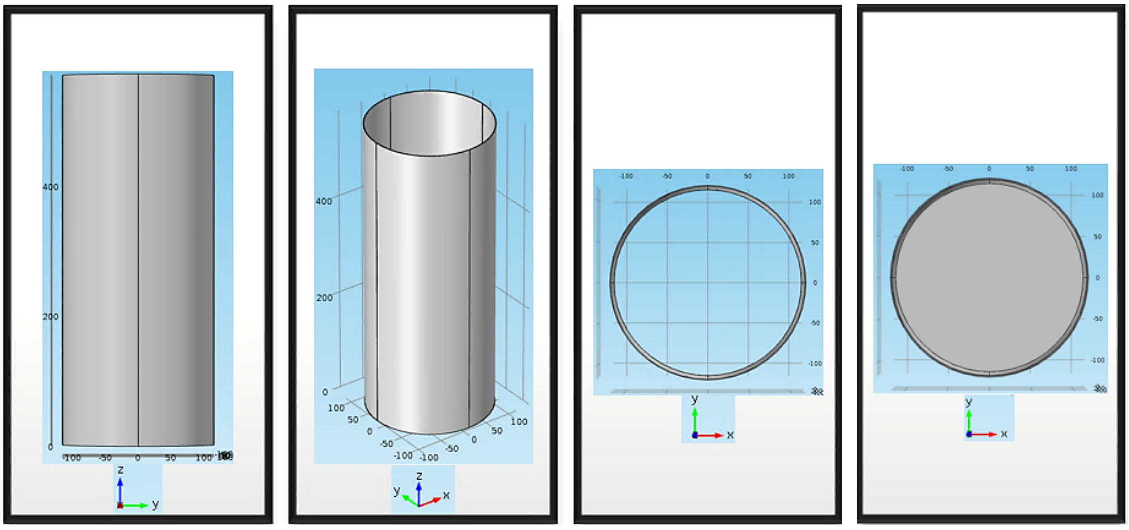

a) **b)**

Figure 11*. Mumetal cylinder simulation, L=575mm D=232,5mm.*
a) *Open cylinder.* ***b)*** *Cylinder with end cap.*

As expected theoretically, the (z-axis) axial shielding factor in the open cylinder has a maximum (S.E. ≈ 79) in the middle. The magnetic flux is entrapped by the end of the cylinder and is directed through the material to the other end, as shown in Figure 10. In contrast, the cylinder with a completely closed end cap shows the maximum shielding effectiveness (S.E. ≈ 118) in the end cup area. As explained before, this means that the end cup provides a low reluctance path to an extra magnetic field that leaks inside the shield. (Figure 12)

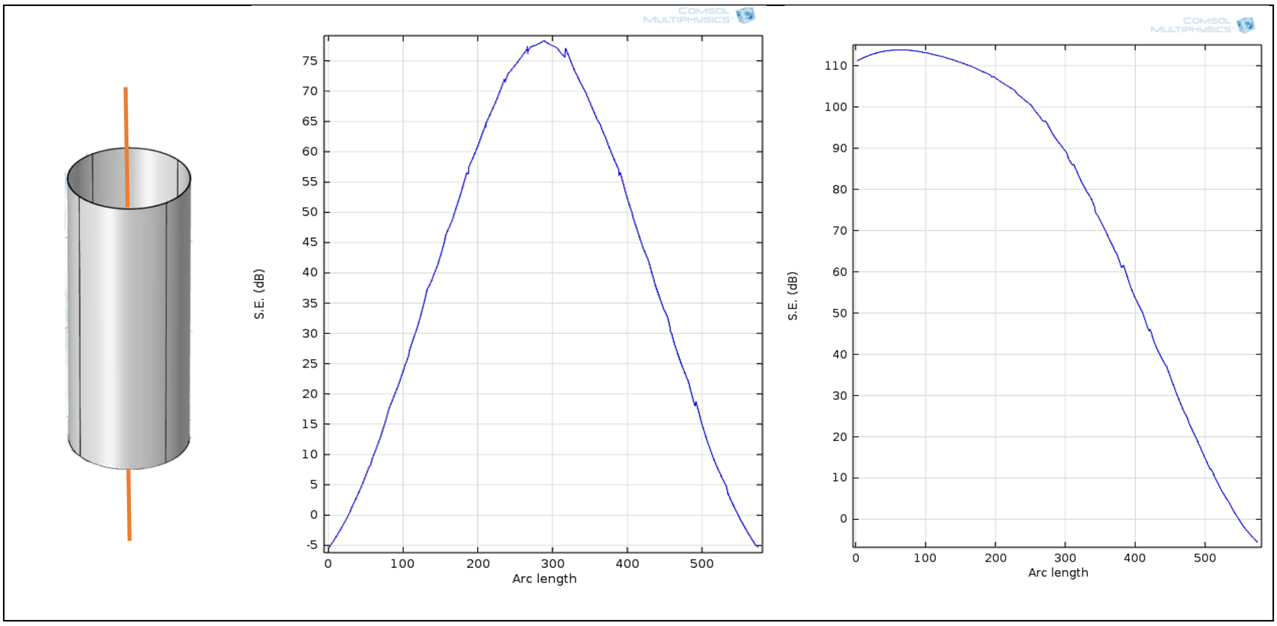

LENGTH **a)** **b)**

Figure 12. *S.E. along the axis (mm) (orange) of Mumetal cylinder simulation, Axial H component.*
a) *Open cylinder.* ***b)*** *Cylinder with end cap.*

The simulation of the (x-axis) transversal shielding factor in the open cylinder continues to have the maximum in the middle of the shield. However, the value of the maximum S.E. has increased (S.E. ≈ 110), and the peak of the graph has been broadened. The end cap cylinder shows also an increasing in the maximum S.E. value (S.E. ≈ 119) and the slope of the transversal graph appears less pronounced than with the axial component. This means that a qubit placed in that closed cylinder will be more protected from possible fluctuations of the field than in the open cylinder case. (Figure 13)

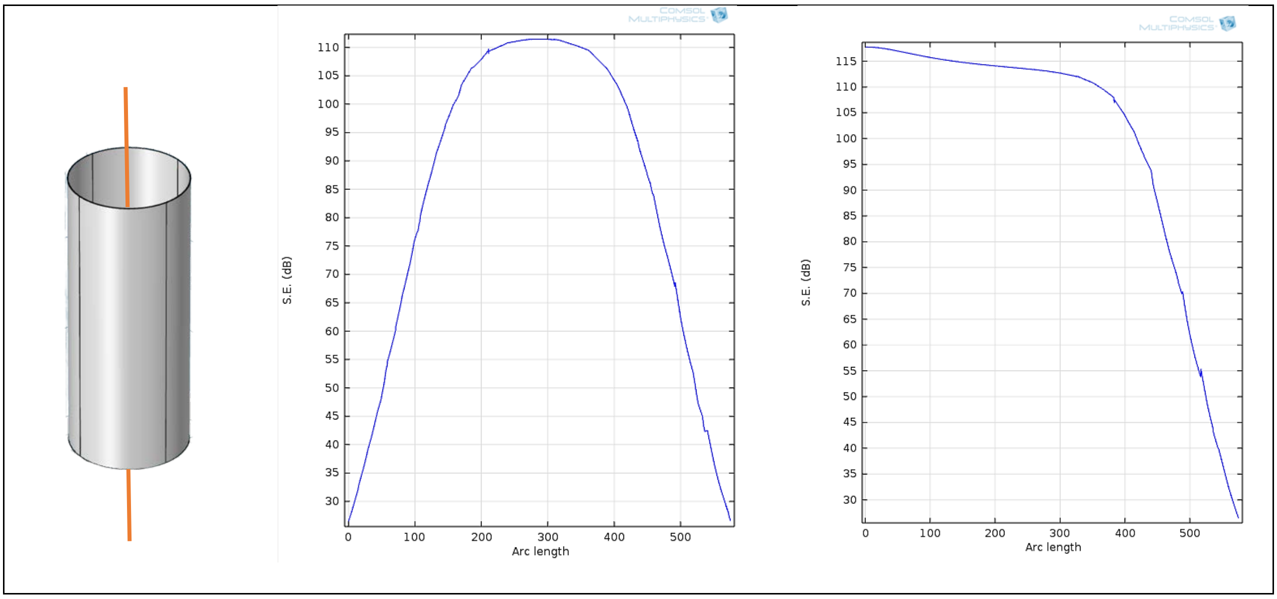

LENGTH **a)** **b)**

Figure 13. *S.E. along the axis (mm) (orange) of the Mumetal cylinder simulation, Transversal H component.*

a) Open cylinder. b) Cylinder with end cap.

The behavior of the cylindrical shield can be explained by the length-to-diameter aspect ratio:

$$\mathrm{AR} = \frac{Length}{Diameter}. \tag{3.2}$$

A cylinder with uniform thickness and large aspect ratio shows a higher shielding factor in the transverse direction than in the axial direction. [21]However, as in this case AR = 2.47, the difference is not very large.

As the qubit will be placed on the “Experiment” area in Figure 9, the geometry most suitable is the cylinder with a completely closed end cap, based on both theorical and simulation results.

3.2.1.2. End cup angle study

Having decided that the Mumetal cylinder would have an end cup, and motivated by an article studying different geometries[25] , the following question came up: Would the shielding factor increase if the end cap had another geometry?

The first try was to simulate a Mumetal cylinder with a conical end cap. The result of the S.E. vs length with both transversal and axial components was compared by decreasing the bottom radius, as shown in Figure 14.

In order to favour the visualization of the shielding effectiveness, the S.E. equation (3.1) was used without the negative sign.

R_B = 20 mm

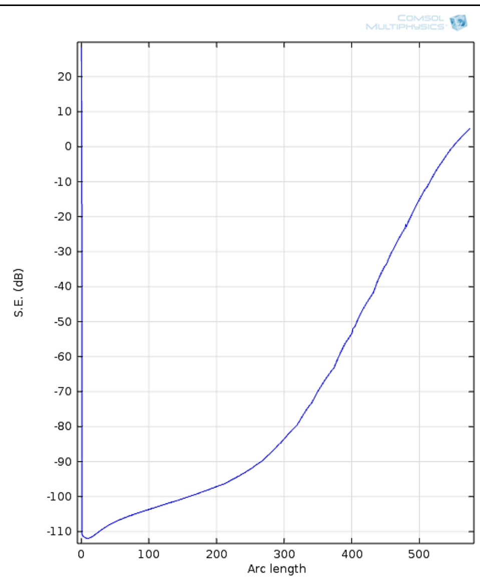

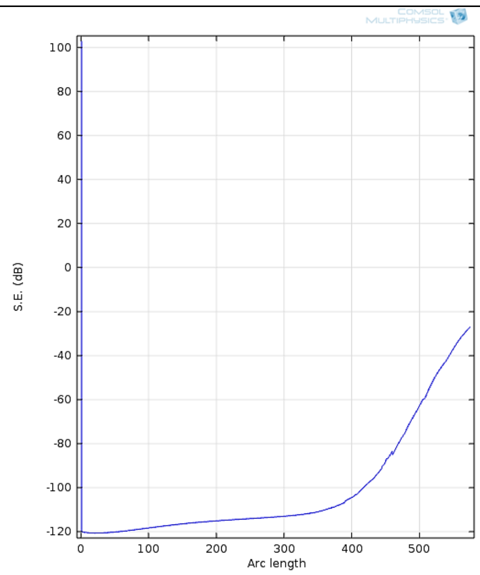

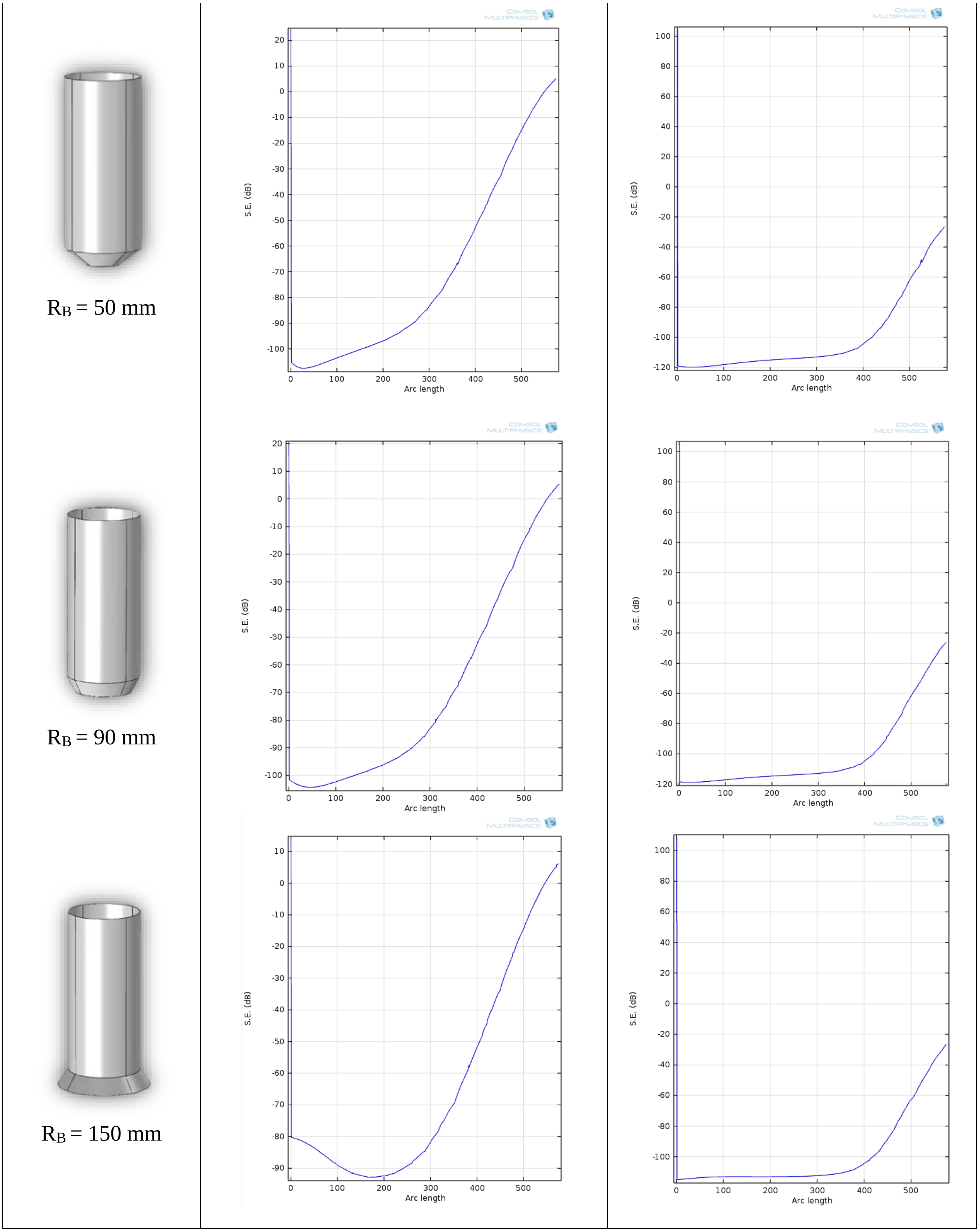

LENGTH **a)** **b)**

Figure 14. *S.E. along the central axis (mm) of the Mumetal cylinder simulation, Bottom angle variation*
a) *Axial H component* ***b)*** *Transversal H component*

The results (Figure 14) show a significant change in the axial shielding factor compared to the transverse one. An absolute minimum appears for R_B = 150 mm, around the area where the qubit would be placed. Moreover, the transverse shielding plot using this bottom radius value, has a less pronounced slope compared to the other plots.

More simulations were performed with larger radius values in order to obtain an axial shielding with a less pronounced minimum that would translate in less fluctuations of the field if the qubit position was to fluctuate. This fact was more relevant that the slight difference between slopes (S_{150}=0.4, $S_{122,58}$=0,5). The best results were obtained with R_B = 122,58 mm, the bottom radius that would be used in our “warm” magnetic shield. (Figure 15)

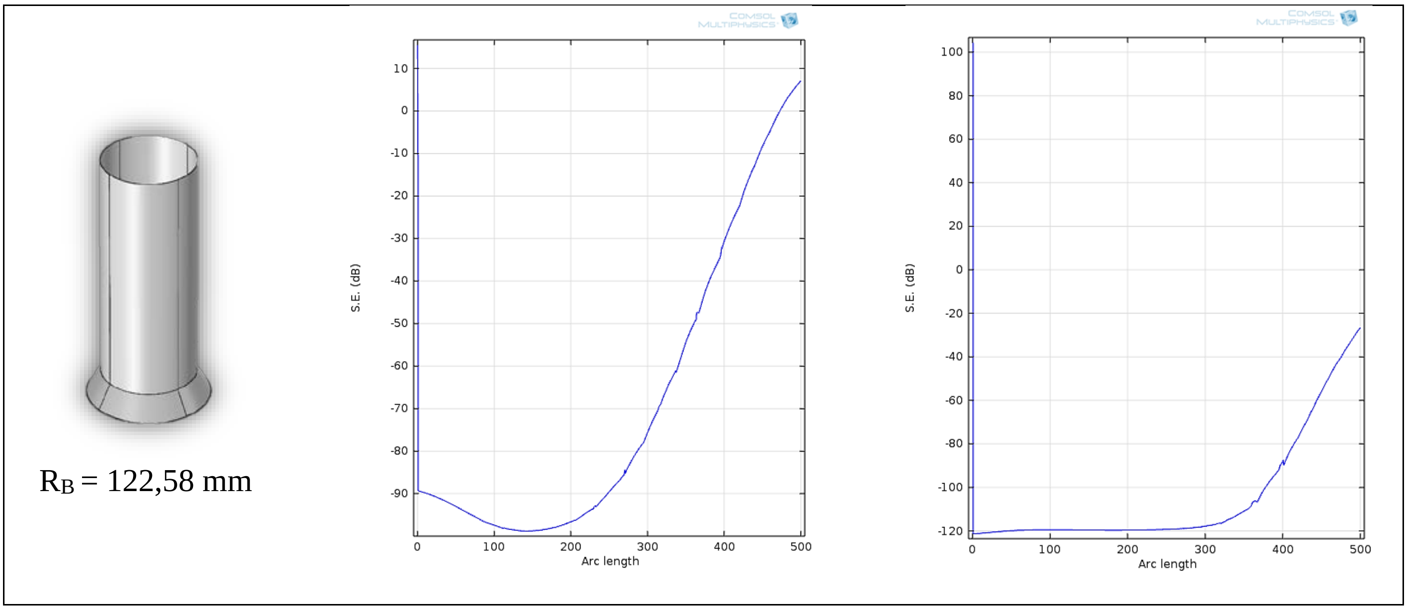

a) **b)**

Figure 15*. S.E. along the central axis (mm) of the Mumetal cylinder simulation,* <u>R_B = 122,58 mm</u>
a) <u>*Axial H component*</u> ***b)*** <u>*Transversal H component*</u>

3.2.1.3. Final geometry

After having the laboratory’s construction drawings, a modification on the cylinder length had to be made. The new length was L = 995mm.

Without modifying the rest of parameters, the simulation was performed to observe the effect of increasing the length in the shielding effectiveness. Although the graph showed a similar tendency to the previous one, the S.E. had decreased, as shown in Figure 16.

As a solution, the length of the end cap was increased with respect to the rest of the cylinder. Now, instead of having L=895+100mm, a new simulation with L=845+150 mm was performed. (Figure 16)

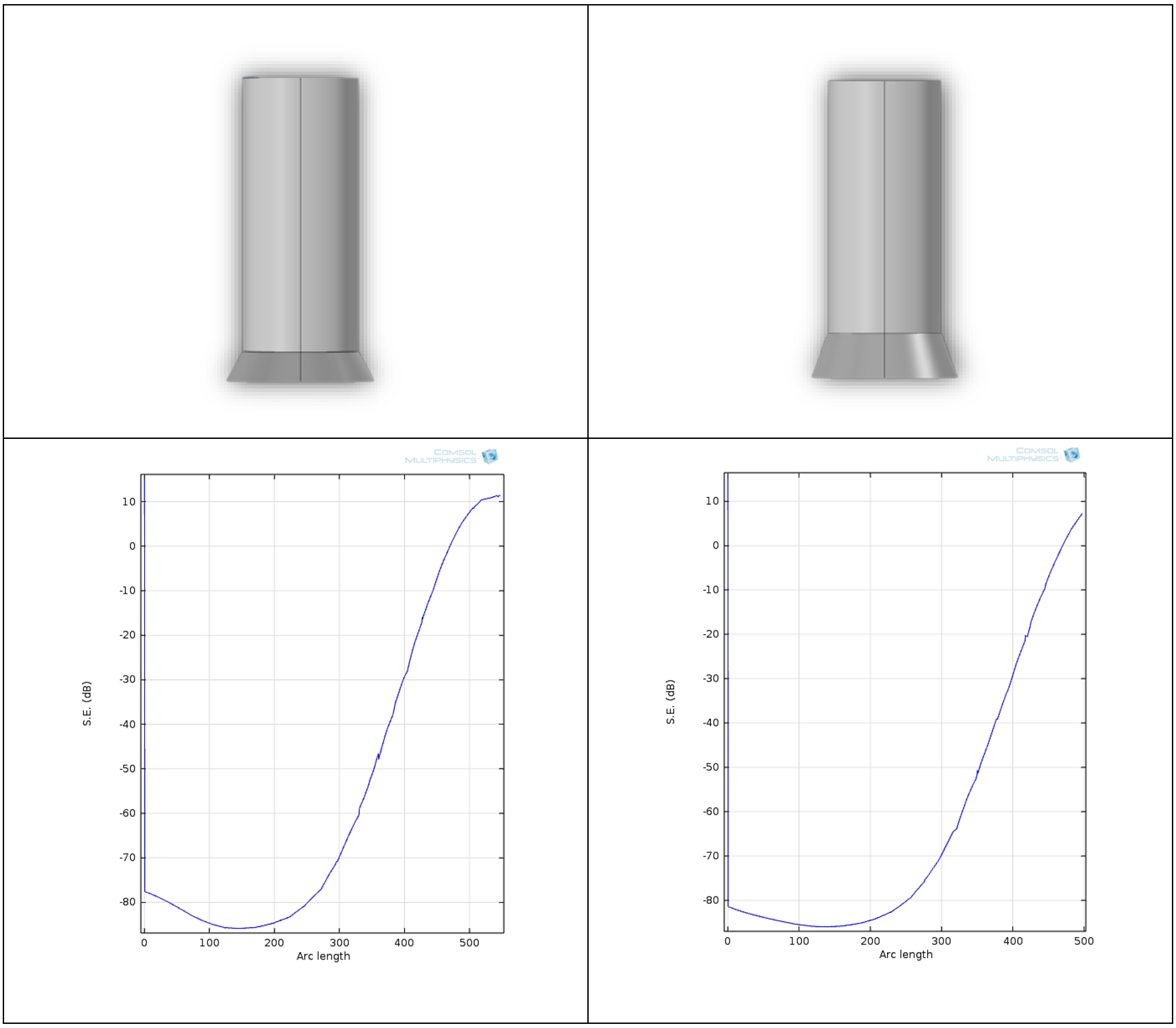

a) ***b)***

***Figure 16**. S.E. for the axial component along the central axis (mm) of the Mumetal cylinder simulation, R_B = 122,58 mm*

a) *100mm end-cap* ***b)*** *150mm end-cap*

The new geometry met both requirements: having a less pronounced minimum and a high value of S.E., as shown in Figure 16. This geometry was finally decided to be used for the Mumetal magnetic shied.

3.2.2. Cryophy simulation

The Quantum Computing Technology research group uses a superconducting aluminum cavity to protect the qubit from the environment. The cavity with the qubit inside is held at a temperature below 25mK, by using a ^3He-^4He dilution refrigerator. [26] The cryogenic environment influences the magnetic properties of materials. However, magnetic shielding materials have been designed for use at this temperature.

A "cold" shield inside the fridge made of Cryophy [18] is studied in this section.

Cryophy[18], a registered trademark of Aperam, is a Ni-based ferromagnetic alloy, primarily composed by 81% Iron, 14% Niquel and 5% Molybdenum by weight. In contrast with Mumetal, whose permeability decreases by decreasing the temperature, Cryophy has the property that instead of decreasing, its permeability increases at low temperatures. The permeability used in the simulation was $\mu_r = 7 \cdot 10^4$.[18]

The idea was to design a geometry of a superconducting aluminum shield that would be placed inside the cryostat, as will be explained in the "3.2. Superconducting materials" section, shown in Figure 17.

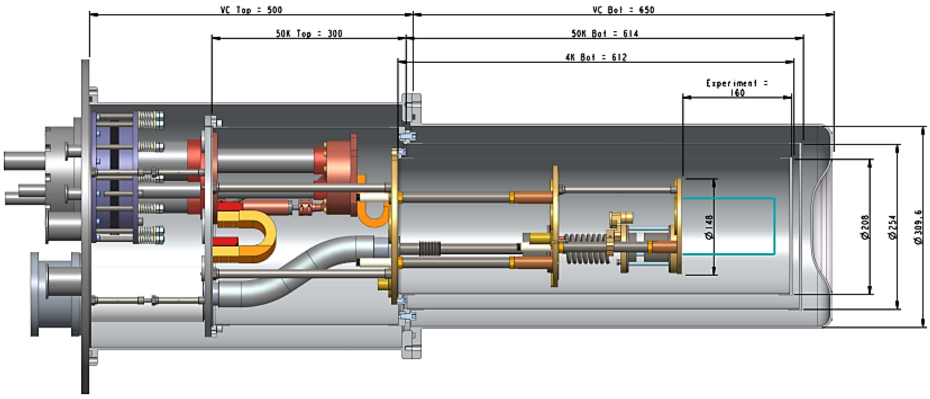

Figure 17. *Blue: Cryophy shield placed at cryostat from the Quantum Computing Technology group.*

A first bottle geometry was simulated and compared with a flat end-cap cylinder, as had been done with the Mumetal shield (Figure 18). The parameters were length L = 140mm, diameter D = 60mm and thickness t = 1mm (also a small diameter d = 24, 34mm). However, in this case, the behaviour of the axial shielding effectiveness outside the geometry was also studied and compared between both geometries (Figure 18).

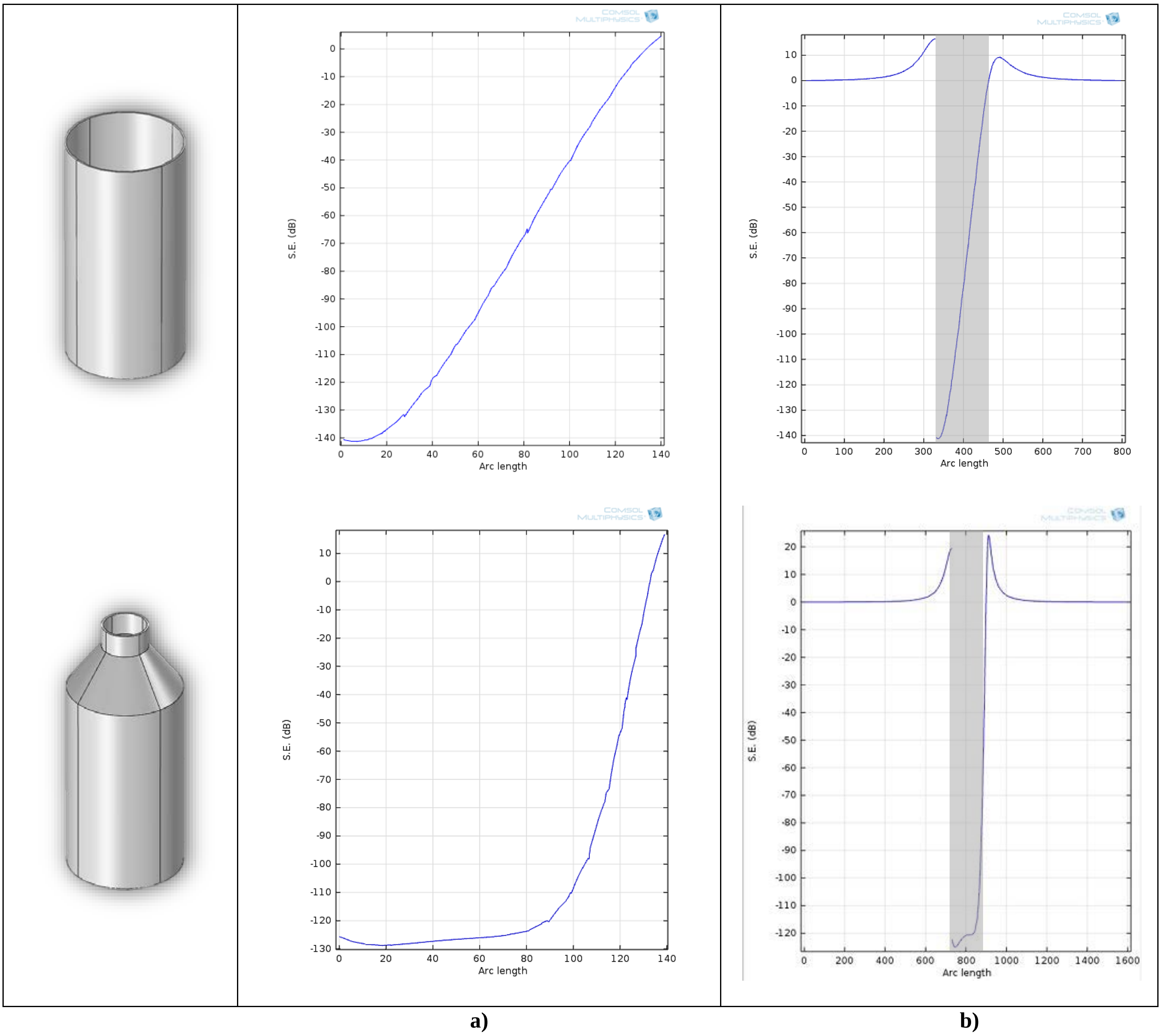

Figure 18. *Axial S.E. along the central axis (mm) of the Cryophy geometry. Flat endcap vs Bottle geometry.* ***a)*** *Inside the geometry* ***b)*** *Inside(grey)+Outside the geometry*

Although having a less maximum in absolute value of S.E., the bottle geometry shows a clear constant shielding compared to the flat end-cap as function of depth. As shown in Figure 18, there is a discontinuity between the outside and inside regions, which matches with the place of the end-cap. This feature appeared every time an outside simulation of a geometry with endcaps was performed.

Due to the favourable results, the bottle geometry was chosen to be the Cryophy magnetic shield geometry.

3.3. Superconducting materials

Aluminum is the superconducting material studied in this project.

Lead was also considered to be one of the shields used. Because of its properties, such as density and high atomic number, lead is very effective at shielding gamma and x-ray radiation. However, although lead is an effective method to protect from magnetic fields and high-energy particles, it was no considered due to its high radioactivity. De-activated lead would be an ideal alternative, but it is not available commercially.

Magnetostatics involving a superconducting material can be modeled by assigning a relative permeability $\mu_r = 0$. However, as said before, this value cannot be used and was approximated by using $\mu_r = 10^{-6}$.

3.3.1. Aluminum simulation

Aluminum has an excellent low-temperature electrical conductivity, low heat capacity during cooldown and low density. [27] In fact, Al is a conventional type I superconductor which becomes superconductor at 1.18K. [28]

A high magnetic shielding efficiency is related to completely closed superconducting. However, the presence of holes for connecting wires makes the magnetic field fall off inside the shield with a distance x from the opening.

In order to reduce the penetration of the external magnetic field inside the shield, a magnetic shield could be used outside the superconducting shield.

The structure in Figure 19 was designed to place the Cryophy bottle inside, with L = 150mm, D = 140mm and t = 1mm. Holes were needed to allow wires to reach the superconducting qubit.

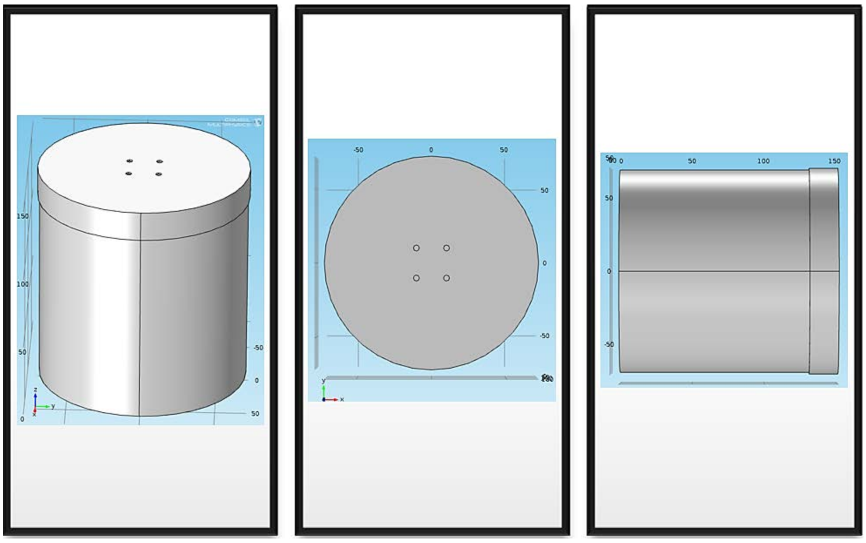

Figure 19*. Aluminum geometry simulation. Length L=150mm, diameter D=140mm, thickness t=1mm*

The axial shielding effectiveness inside and outside the geometry was simulated, as shown in Figure 20.

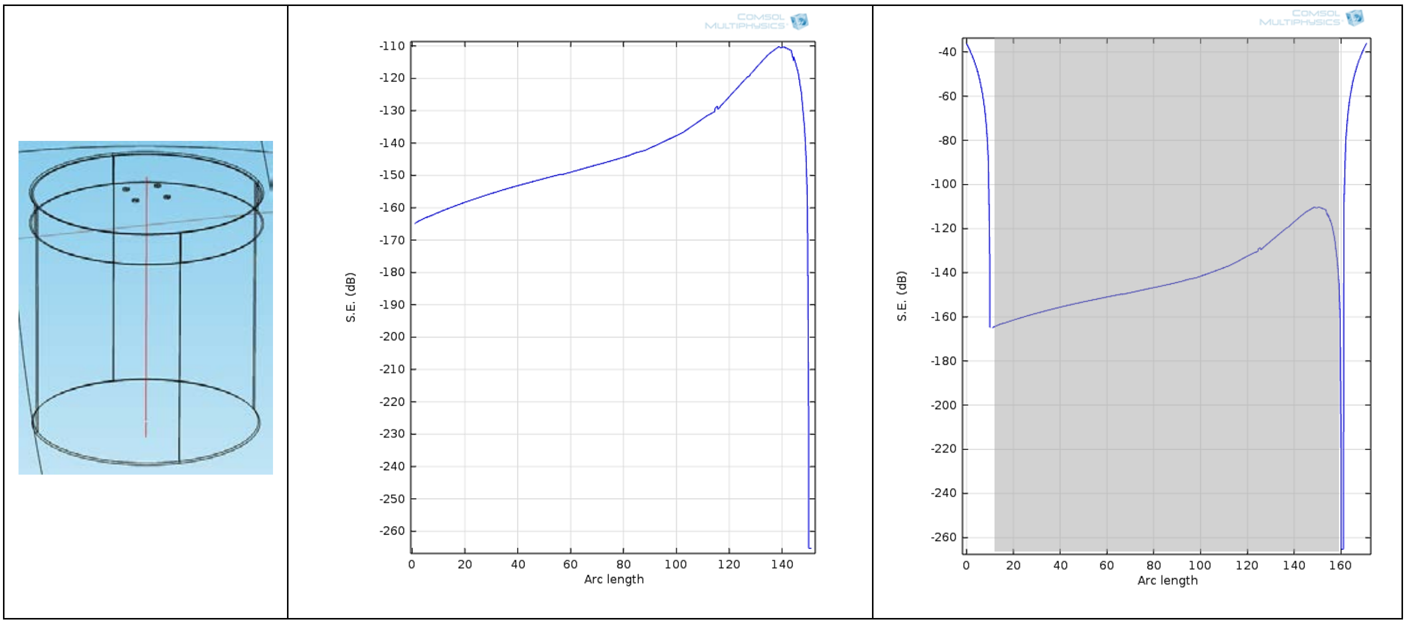

a) b)

Figure 20. *Axial S.E. along the length of Cryophy geometry. Inside vs Inside+Outside.*
a) *Inside the geometry* ***b)*** *Inside(grey)+Outside the geometry*

In order study the behaviour of the magnetic field inside the holes, this simulation of the shielding effectiveness was also performed through one of the holes, as shown in Figure 21.

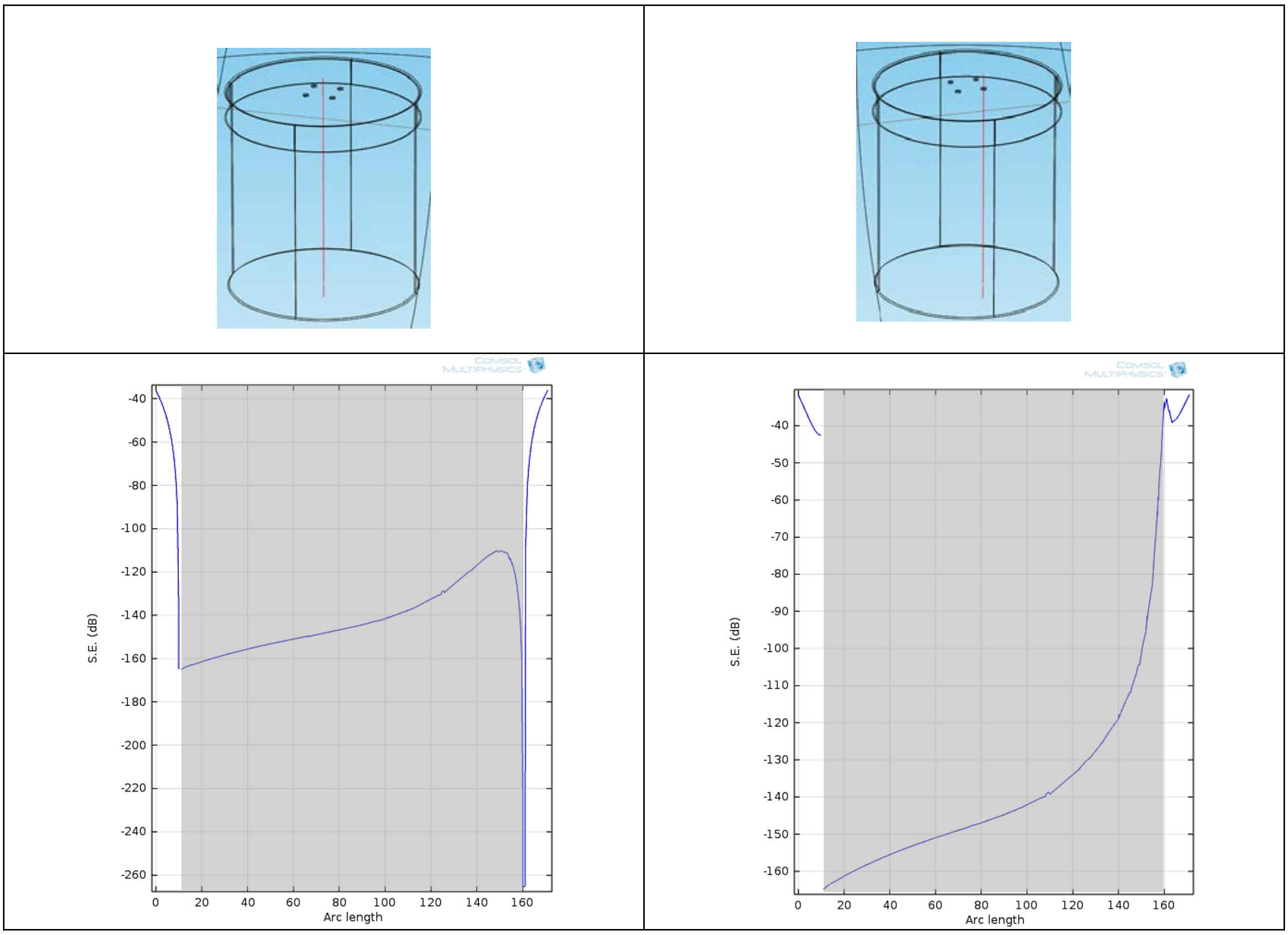

b) ***b)***

Figure 21. *S.E. along the length of Aluminum shield simulation*
a) *Middle of the geometry* ***b)*** *Through a hole*

As can be seen, the shielding effectiveness along the middle of the geometry has a large maximum in the middle of the holes, arriving to |S.E.| ≈ 270. In contrast, the simulation performed along the hole shows the minimum value where the hole is placed of |S.E.| ≈ 30. This can be explained because the magnetic flux remains trapped in the holes, resulting in a large magnetic shielding in the space between the four holes. The effect of a hole is comparable to that in high-μ materials.

The effect of the holes was also compared to the simulation along the middle of the aluminum geometry with and without holes in the cap, as shown in Figure 22.

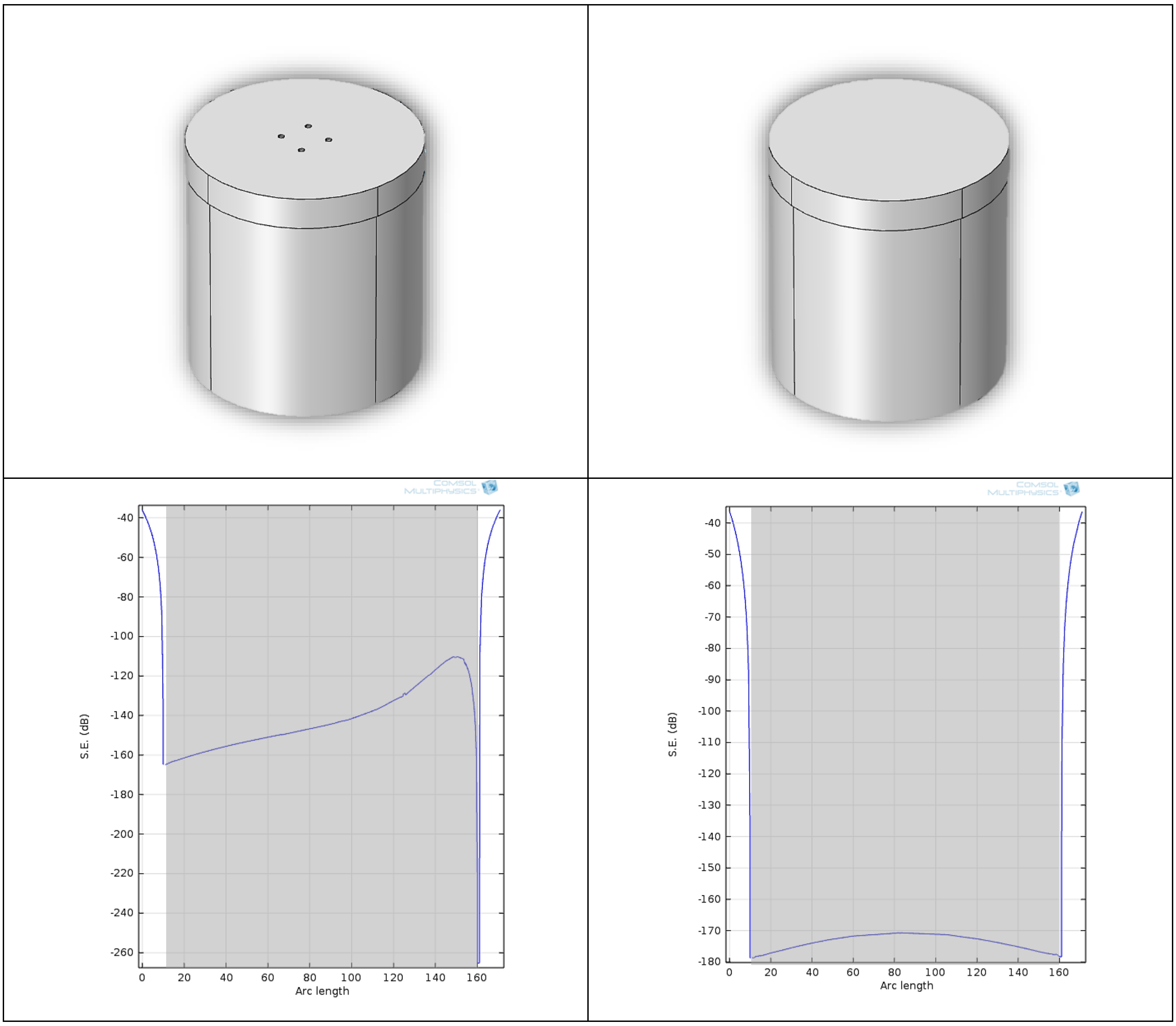

a) ***b)***

Figure 22*. S.E. along an axis of Aluminum shield simulation*
a) *<u>Middle of the geometry</u>* ***b)*** *<u>Through a hole</u>*

Comparing both graphs, the one without holes clearly confirms that the maximum peak seen in simulation of the geometry with holes, is because of the presence of holes. There is no penetration from the small gap existing for the short cap without holes. Moreover, the increased shielding occurs in the vicinity of both caps.

3.4. Final simulation: Matryoshka

In this section, I would like to summarize the final order for the high-μ and superconducting shields that have been studied. For this purpose, the order of the materials is going to be explained, starting from the smallest one, which will have the superconducting qubit inside.

An ideal superconductor would expel all external magnetic field due to Meissner effects. However, the magnetic field can be trapped in impurities or inhomogeneities while the critical temperature T_c is reached. Because of that, the magnetic field at the surface need to be minimized before arriving to the T_c. Below T_c, magnetic fields are effectively screened.[29]

To ensure that the superconducting shield act as a zero-field shielding region, the superconducting shield itself has to be cooled down in a zero-field environment.

The first idea was to shield the superconducting qubit using a high-μ material, the Cryophy one. This "cold" magnetic shield would also be inside a superconducting aluminum shield, as shown in the Figure 23.

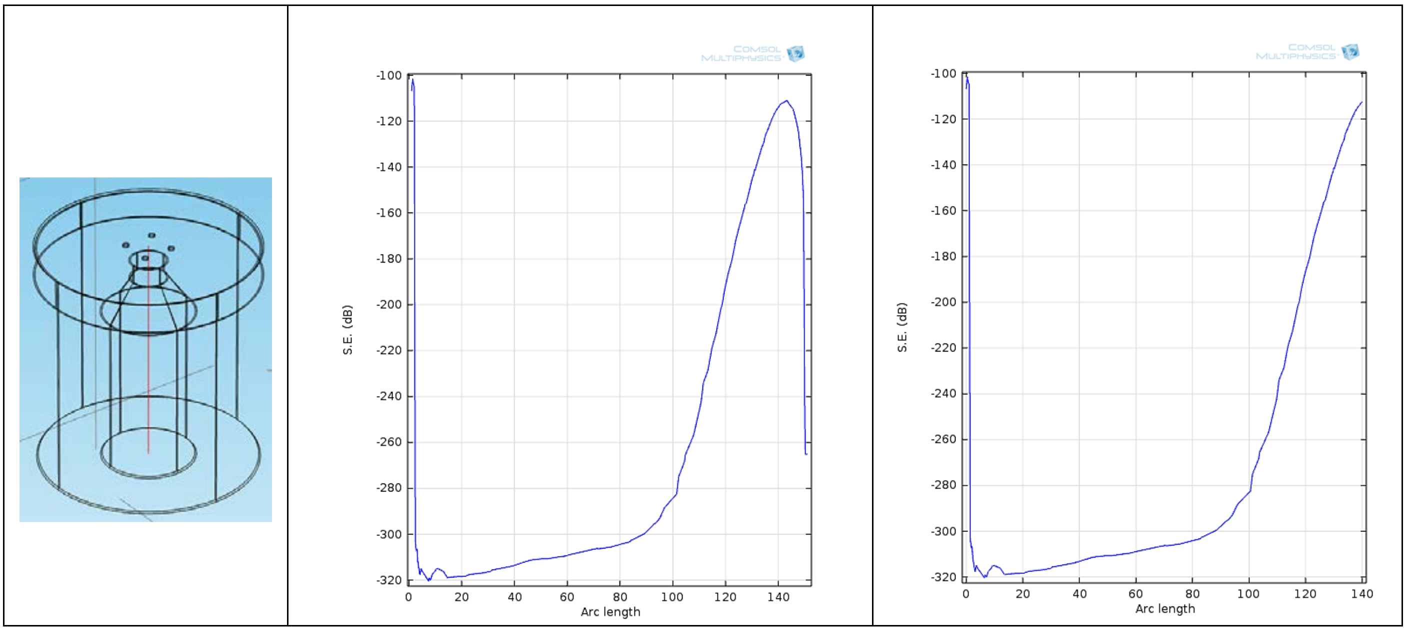

a) b)

Figure 23. *Axial S.E. along the central axis (mm) of the Aluminum and the Cryophy geometry.*
a) *Inside the Aluminum shield* ***b)*** *Inside the Cryophy shield*

The result shielding factor is a sum of both geometries separately. Although this result was promising, the reverse order was decided, the experimental conditions require the reverse order to be applied, using the aluminum shield inside the Cryophy one. In this way, the superconducting shield would reach its T_c in a low-field environment, avoiding magnetic flux trapped in the form of vortexes*.

The outermost shield, as seen before, is the Mumetal shield. With the aim to study the shielding effectiveness of both high-μ shields, Mumetal and Cryophy, the simulation shown in Figure 25 was carried out. The Cryophy's parameters were reduced by half, as the ones of the Mumetal shield (Figure 24).

(*) The reverse simulation could not be performed, due to the COVID-19 situation.

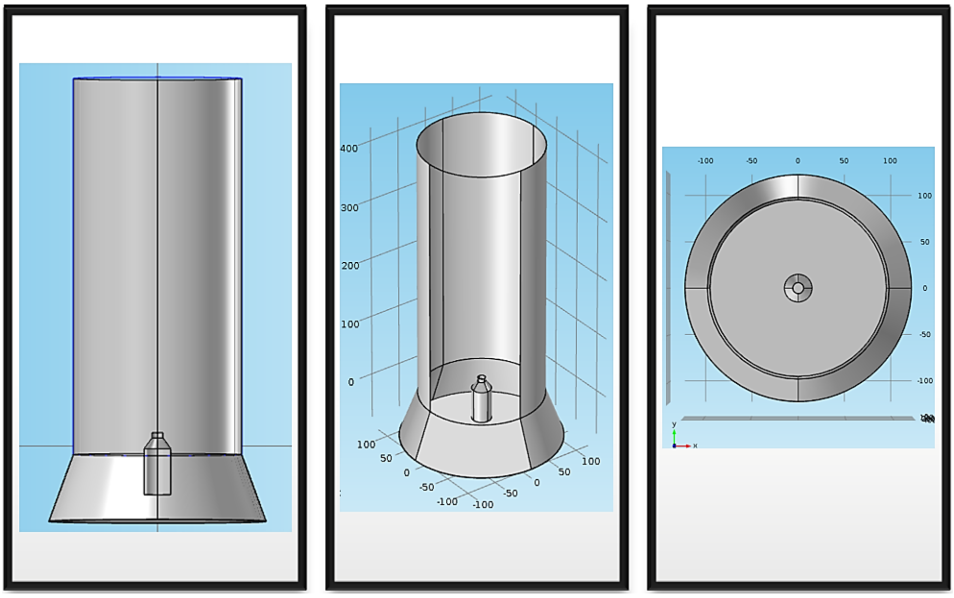

Figure 24*. Mumetal and Cryophy geometry simulation.*
Mumetal: L=497,5mm, D=190mm, t=1mm
Cryophy: L'=70mm, D'=30mm, t=0.5mm

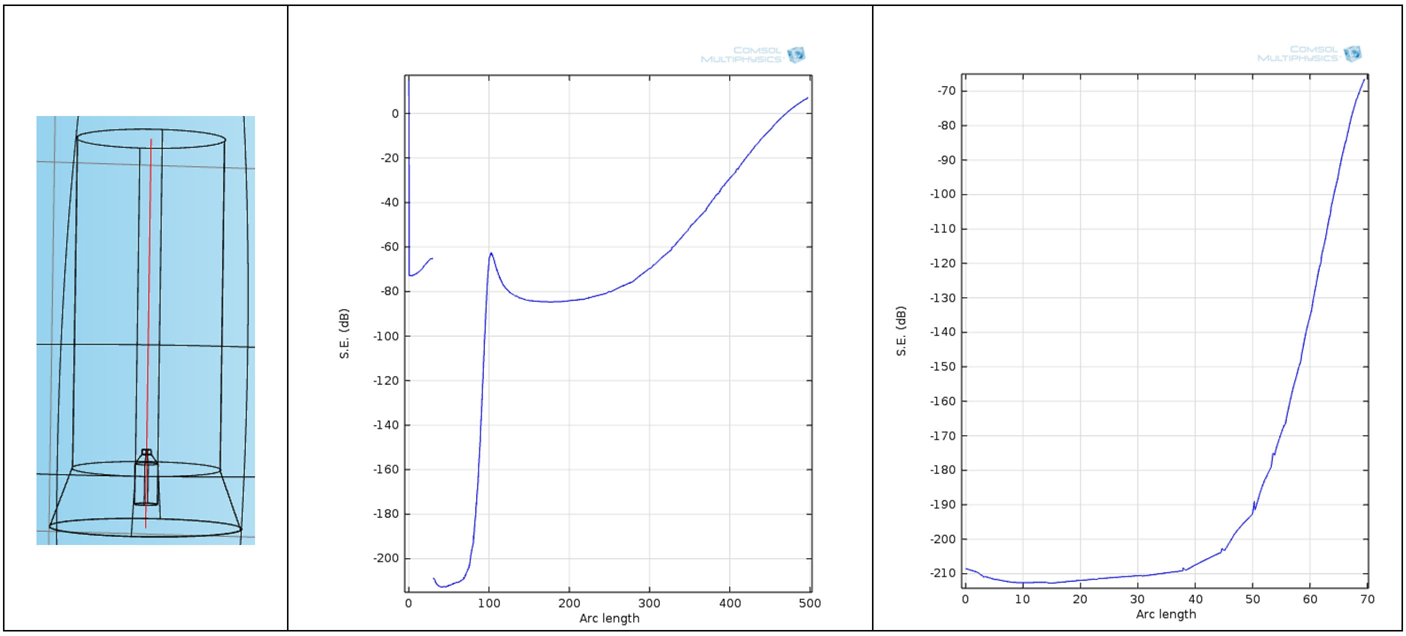

a) **b)**

Figure 25*. Axial S.E. along the length of Mumetal and Cryophy geometry.*
a) *Inside the Mumetal shield* ***b)*** *Inside the Cryophy shield*

In conclusion, the final order of the magnetic shields is illustrated in Figure 26. The project Matryoshka is the result of combining superconducting and high-μ materials, making use of characteristics of both materials to achieve the best magnetic shielding. A high shielding factor and a less pronounced minimum of the S.E. vs length in the qubit region are the key points.

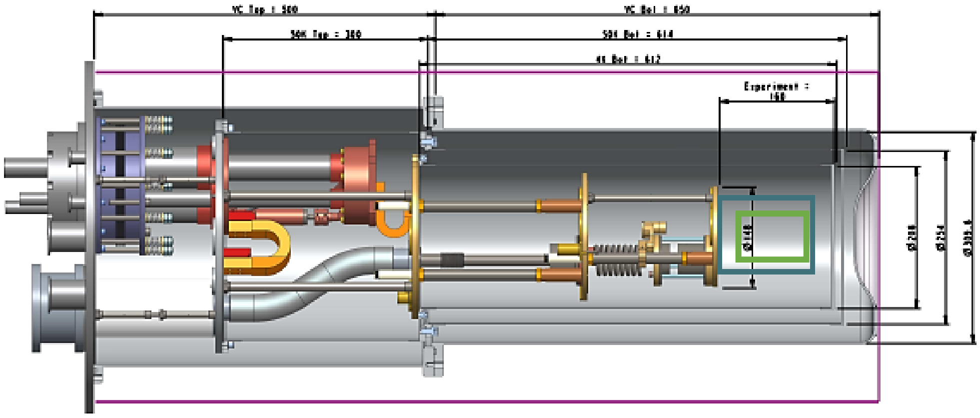

Figure 26. *Matryoshka design placed at cryostat from the Quantum Computing Technology group. Purple: Mumetal shield, Blue: Cryophy shield, Green: Aluminum shield.*

CHAPTER 4: CONCLUSION AND NEXT STEPS

The main goal of this project was to find the best combination of high-permeability and superconducting materials, as well as the most effective geometry for each of them, to achieve the highest magnetic shielding for superconducting qubits.

Establishing an optimal configuration of thickness, size, shape, permeability and number of layers is essential to maximize the shielding effectiveness. Also, some problems such as the presence of holes could decrease the shielding factor by providing a path for the magnetic flux to enter the space to be shielded. Consequently, several simulations were performed using COMSOL Multiphysics.[13]

As shown in chapter 3, first of all, the different materials were studied separately in order to compare the obtained results with the theory (Ch.2). Mumetal[17] and Cryophy[18] were the high-permeability materials studied as warm and cold passive magnetic shield, respectively. Aluminum was the chosen superconducting shield, inside which the superconducting qubit will be placed.

Secondly, using the same software, the best geometry results obtained previously, were simulated. Taking into account several parameters such as the different temperatures of the cryostat or the behavior of the materials with temperature, the order of the shields was decided.

In order to expedite the Mumetal simulation, the size of the geometry was reduced by half. As shown in the Annex C, varying proportionally the size does not result in scaled results, due to the lack of symmetry in the studied case.

The simulation results showed a different shielding of the axial and transversal field components. As the transveral component is more attenuated than the axial and causes less fluctuations, the qubit should be preferably placed perpendicular to the shield axis.

However, the future idea is to place several simultaneous experiments inside the cryostat. Using a Cryophy shield with an Aluminum shield inside, as studied here, could be used, but the possible interference between the superconducting qubits as well as the size of the shields needs further investigation.

The simulation results were going to be compared with experimental results, since the Mumetal geometry was built and placed on the Quantum Computing Technology laboratory. However, the comparison was not possible due to the COVID-19 situation.

ACKNOWLEDGEMENT

As the final words of the project, I would like to dedicate these words to the people who directly, indirectly or both, have been part in this **experience**.

Firstly, I would like to thank **Dr. Pol Forn-Díaz** for giving me the chance to learn and discover what means to be part of a research group dedicated to the impressive **quantum computing** field. The **Quantum Computing Technology** group is formed by amazing people, with whom I have learned invaluable lessons. I would like to highlight the support from **David López** during all my project, as well as the generosity from **Dra. Gemma Rius**, who did not hesitate to offer me a place on the ICMAB-CSIC to perform my simulations. Thanks to **Xabier Oyanguren** and **Queralt Portell** for giving me the smiles that encouraged me so much.

Secondly, I want to thank my **friends** for their unconditional support and for all those moments that gave me the energy which I needed to keep going. This project could not have done without the encouragement form my **nanotechnologist** colleagues. However, I also want to highlight my best friends, practically relatives, **Isabel Sánchez** and **Jordi Monzonís**, who have always been by my side. I can not forget about **Alba Flores**, thanks for being my ray of light.

Last but not least, I am extremely grateful for the support and motivation from my **family**. In particular, I would like to highlight the name of my grandmother, **Asunción Mayayo Catalán**, to whom I dedicate this project.

Figures

[1] Marijike Antonia Fagan-Endres, “Fundamental studies of heap leaching hydrology using magnetic resonance imaging”, 2013

[2] David Young, “Introduction to Magnetochemistry”, Cytoclonal Pharmaceutics Inc.

[3] Matthew N.O. Sadiku, “Elements of Electromagnetics” 4th Edition

[4] V.V. Schmidt, P.Müller and A.V.Ustinov, “The Physics of Superconductors: Introduction to Fundamentals and Applications”

[5] R. Flükiger, “Overview of Superconducting and Challenges in Applications”, 2012

[6] A. Rettaroli, “Characterization of superconducting resonant RF cavities for axion search with the QUAX experiment”, 2018

[7] Edda Lína Gunnarsdóttir, “The Earth’s Magnetic Field”, Physics Department Háskóli Íslands, 2012

Bibliography

[0] Michael A. Nielsen and Isaac L. Chuang, “Quantum Computation and Quantum Information”, 2010

[1] A. Schneider, T.Wolz, M.Pfirrmann, M.Spiecker, H.Rotzinger, A.V.Ustinov and M.Weides, “Transmon qubit in a magnetic field: Evolution of coherence and transition frequency”, 2019

[2] I.R. Harris and A. J. Williams, “Magnetic Materials, Materials science and engineering”,
Vol. II, 2009.

[3] Soshin Chikazumi, “Physics of Ferromagnetism”, Oxford Science Publication, 1997

[4] Lesley E. Smart and Elaine A. Moore, “Solid State Chemistry”, 2012

[5] Amumetal and A4K, Amuneal Manufacturing Corporation.

[6] CryoPerm, The MuShield Company.

[7] P.Arpaia, M.Buzio, O.Capatina…, “Effect of temperature and mechanical strain on Ni-Fe alloy CRYOPHY for magnetic shields”, 2019

[9] Reinhold Kleiner and Werner Buckel, “Superconductivity: An Introduction”, 3rd Edition

[10] R. Flükiger, “Overview of Superconducting and Challenges in Applications”, 2012

[11] A. C. Rose-Innes, “Introduction to superconductivity”, Elsevier, 2012

[12] J. Koch, T. M. Yu, J. Gambetta…, “Charge-insensitive qubit design derived from the Cooper pair box,”, 2007.

[13] COMSOL, “Introduction to COMSOL Multiphysics”

[14] J.N. Reddy, “An Introduction to the Finite Element Method”, McGraw-Hill, 1984

[15] P. Vanderbemden, J.H. Durrell, D.Zhou, “Bulk superconductors”, 2018

[16] O. Romero-Isart, C.Navau, A.Sanchez…, “Superconducting Vortex Lattices for Ultracold Atoms”, 2013

[17] Magnetic Shield Corporation, “MuMetal Alloy for Fabricated Shields”, 2012

[18] CRYOPHY, Aperam. URL: https://www.aperam.com/sites/default/files/documents/2018-01/Strip_CRYOPHY.pdf

[19] Magnetic Shield Corporation, “Technical Data”, 2015. URL: http://www.mu-metal.com/technical-data.html

[20] MuShield, “Designing A Magnetic Shield”. URL: https://www.mushield.com/magnetic-shielding/#design-magnetic-shield

[21] T. Rikitake, “Magnetic and Electromagnetic Shielding”, 1987.

[22] Anthony C. Crawford, “Magnetic Shielding Properties of a Fermilab International Linear Collider (ILC) Cryomodule”, 2014

[23] B.Feinberg and H.Gould, “Placed in a steady magnetic field, the flux density inside a permalloy-shielded volume decreases over hours and days”, 2018.

[24] F.F.Mazda, “Power Electronics Handbook: Components, Circuits and Applications”, 2013

[25] S. Malkowski, R.Y. Adhikari, J.Boissevain…, “Overlap Technique for End-Cap Seals on Cylindrical Magnetic Shields.”

[26] R. Luque Merino, “Thesis: Coherent control of a superconducting quantum bit”, 2019

[27] M.Young, E.Gregory…”Fabrication and Properties of an Aluminum-stabilized NbTi multifilament superconductor”, 1978

[28] D.U.Gubser and A.W.Webb, “High-Pressure Effects on the Superconducting Transition Temperature of Aluminum”

[29] V. Yashchuk, S.K Lee and E.Paperno, “Magnetic Shielding”, 2012

[30] COMSOL, “AC/DC Module. User’s Guide 5.4”

[31] Stratton J., “Electromagnetic Theory”, 1941

[32] Richard P. Feynman, Robert B. Leighton and Matthew Sands, “The Feynman Lectures on Physics, Vol.II”, 2011

[33] Karttunen, H. et al. Fundamental Astronomy. Springer, 2007.

[34] William Lowrie, “Fundamentals of Geophysics”, 1997

[35] Edda Lína Gunnarsdóttir, “The Earth’s Magnetic Field”, Physics Department Háskóli Íslands, 2012

ANNEX A: COMSOL: MAGNETIC FIELDS, NO CURRENTS.

COMSOL Multiphysics [13] with AC/DC module is a useful tool to design simple and complex 2D and 3D designs, in order to study the effect of geometric factors on the distribution of an applied magnetic field. The outcomes of the simulation from a detailed FEM study is the field's distribution data through the geometry. This solution can be used to estimate the shielding effectiveness of the designed magnetic shields.

In this project, COMSOL Multiphysics was used to study the shielding effectiveness of high-permeability and superconducting magnetic shields. For the optimization of the magnetic shields, COMSOL AC/DC module 3D with "Magnetic Fields, No Currents" [30] static field interface, is used. The magnetic shield boundary conditions are designed to the geometry and the efficacy of the magnetic shielding is evaluated based on the distribution of the applied magnetic field outside and inside the shield. The magnetic scalar potential is the dependent variable in this interface and the distribution of magnetic fields can be solved.

Calculations of magnetic fields in COMSOL are based on Maxwell equations [31]:

$$\begin{aligned} &\int \boldsymbol{E} dl = -\int \frac{\partial \boldsymbol{B}}{\partial t} dS\,, \\ &\int \boldsymbol{D} dS = -\int \rho dV\,, \\ &\int \boldsymbol{H} dl = -\int \left(j + \frac{\partial \boldsymbol{D}}{\partial t}\right) dS\,, \\ &\int \boldsymbol{B} dS = 0, \end{aligned} \tag{A.1}$$

where $\boldsymbol{H}$ is the magnetic field vector, $\boldsymbol{B}$ is the magnetic flux vector, $\boldsymbol{D}$ is the bias current vector, ρ is the volume density of exterior charges, j is the current density, S is the surface square and l is the distance.

In addition, the equations for electromagnetic fields includes the material equation:

$$\boldsymbol{B} = \mu_0 \cdot \mu_r \cdot \boldsymbol{H}, \tag{A.2}$$

Where μ_0 is the vacuum magnetic permeability (H/m) and μ_r the medium (material) relative magnetic permeability.

The first step is to define the parameters that will be used in our simulation, such as the magnetic field applied $H = 5 \cdot 10^{-5}\ (T)$. After determining the parameters, the following step is to build the shield and assigning a material to each component of the shield. In this project, we have used homogeneous material shields. Also, an empty space is not a domain, COMSOL does not consider it in the model. Because of that, a vacuum sphere enveloped the shield, as we simulated hollow structures, in order to create a domain that could be meshed.

In "Magnetic Fields, No Currents", the function "Magnetic Flux Density" allows assigning the value of both the background magnetic field and the one of the shield. The background magnetic field corresponds to the parameter $\boldsymbol{H}$. The magnetic field of the shield is determined by using the relative magnetic permeability, which was defined in the material section.

In the following step, the mash must be computed. Using this interface requires a fine mash to acquire a realistic solution. Because of that, each geometry required a different element size for partitioning.

The shielding effectiveness was calculated for the static magnetic field applied along the length (axial field, z-axis) or applied perpendicular to the length of the shield (transverse field, x-axis), by creating a line where the calculations were going to be performed, as shown in Figure 27.

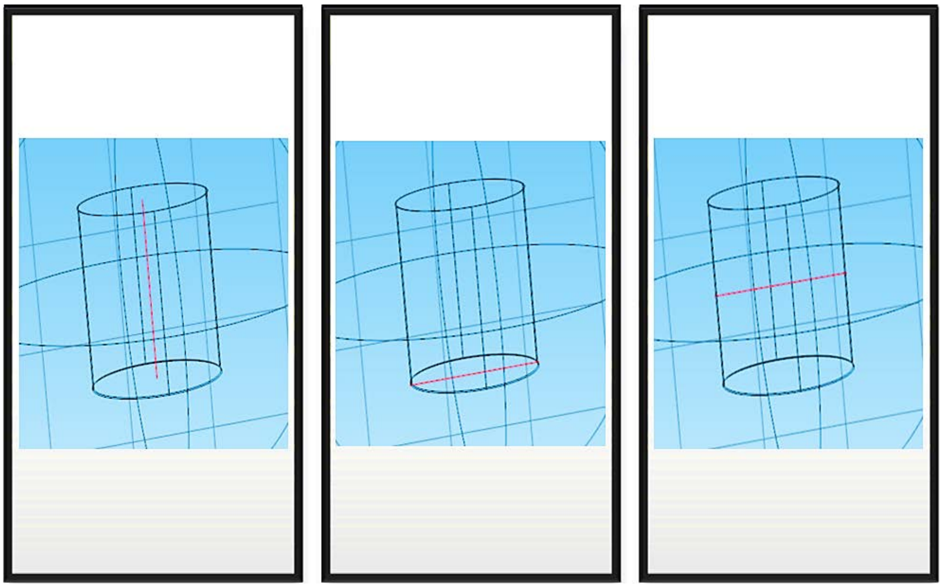

Figure 27*. Red line: Cut line, data set.*

The shielding factor used was:

$$\text{S.E.} = -20 \log\left(\frac{H}{H_0}\right) \tag{A.3}$$

Also, when the simulation has been performed, arrow plots can be used to visualize field distributions, as shown in Figure 28.

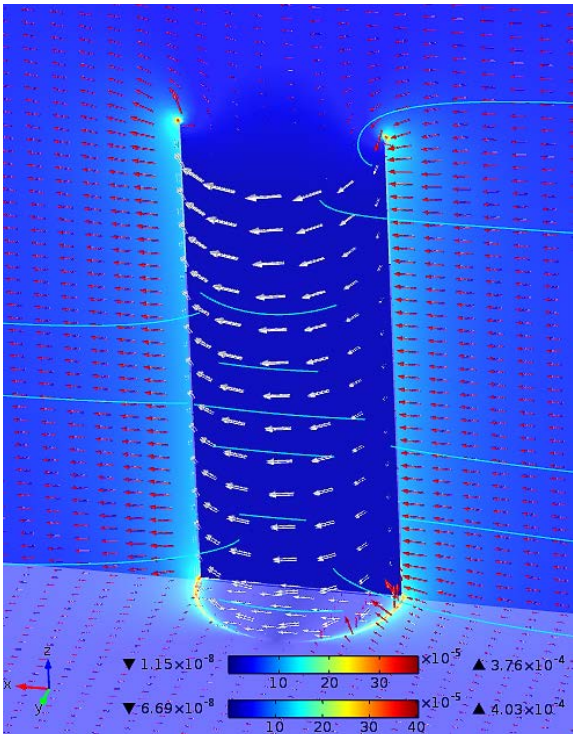

Figure 28*. Flat end-cap Mumetal cylinder: Representation of the magnetic field.*

ANNEX B: EARTH'S MAGNETIC FIELD

The Earth's magnetic field protects the near-Earth environment from dangerous radiation and high energy plasma from the Sun by partially blocking out. This field forms a protecting shield around the planet called magnetosphere.

The observed magnetic field on Earth is called geomagnetic field, which is a superposition of magnetic fields produced by a wide variety of sources. The largest contribution has an internal origin, the main/core field and the crustal field, which is produced by magnetized rocks. The externals magnetic fields are caused by electric currents in the ionosphere and magnetosphere. There is also an induced field, produced by induced currents due to time variations of the main and external fields.

However, as it is practically impossible to perform magnetic measurements for all places on the Earth's surface. The geomagnetic field is described by a model assuming that the field close to the surface, can be described approximately as a dipole field in the Earth's center: The Earth's magnetic field can be approximated as a magnetic dipole, as shown in Figure 29. The intersection points with the Earth's surface define the north and south magnetic poles.

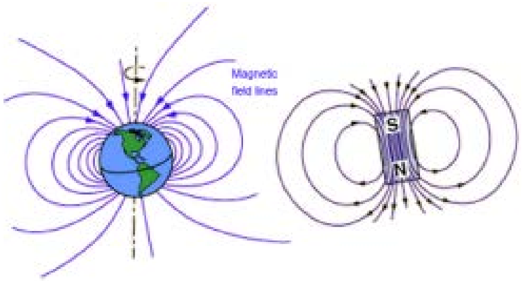

Figure 29. *Earth's magnetic field as magnetic dipole* [7]

To determine the geomagnetic field, the method of spherical harmonic analysis can be used, derived from Laplace's equation. The two Maxwell's equations related to the magnetic field are: [32]

$$\nabla \cdot \boldsymbol{B} = 0 \qquad (B.1)$$

$$\nabla \times \boldsymbol{H} = \mu\left(\boldsymbol{J} + \frac{\partial \boldsymbol{D}}{\partial t}\right), \qquad (B.2)$$

where **H** is the magnetic field, **B** is the magnetic induction, **J** is the electric current density and $\partial \boldsymbol{D}/\partial t$ is the electric displacement density. Equation (B.2) becomes $\nabla \times \boldsymbol{H} = 0$ by using the approximation of no electric currents on the Earth's surface. Consequently, the magnetic field, **H**, is a conservative vector field and can be related to a magnetic scalar potential **V**:

$$\boldsymbol{H} = -\nabla V. \qquad (B.3)$$

The magnetic induction, $\boldsymbol{B} = \mu_0 \cdot \mu_r \cdot \boldsymbol{H}$, becomes $\boldsymbol{B} = \mu_0 \cdot \boldsymbol{H}$ at the Earth's surface.

Combining the previous equations (B.1) and (B.3), Laplace's equation for the magnetic scalar potential is obtained:

$$\nabla^2 V = 0. \qquad (B.4)$$

This equation, assuming the Earth shaped as a perfect sphere, as shown in Figure 30, can be expressed in spherical coordinates:

$$\nabla^2 V = \frac{1}{r^2}\frac{\partial}{\partial r}\left(r^2\frac{\partial V}{\partial r}\right) + \frac{1}{r^2 sin\theta\partial\theta}\left(sin\theta\frac{\partial V}{\partial\theta}\right) + \frac{1}{r^2\sin^2\theta}\frac{\partial^2 V}{\partial\varphi^2} = 0. \qquad (B.5)$$

V(r, θ, φ) is a harmonic function, where r is the radial distance of a point P from the center of the Earth, θ is the angle from the z-axis to the vector and φ is the geographic longitude.

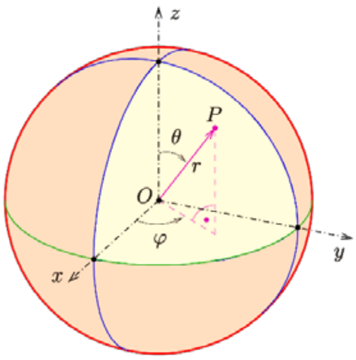

Figure 30. *Earth as a spherical coordinate system.*

The total magnetic potential is the sum of all internal and external potentials, but since the external one on average contribute only about 1-2% to the permanent field, the external potential is going to be considered negligible in comparison to the rest in the following calculation. [33]

Equation (B.5) can be solved by separation of variables, obtaining the scalar magnetic potential caused by currents inside the Earth:

$$V^{internal} = R\sum_{m=1}^{\infty}\sum_{n=0}^{n}\left(\frac{R}{r}\right)^{m+1} P_m^n(cos\theta)(g_m^n cosn\varphi + h_m^n sinn\varphi)\,, \qquad (B.6)$$

where R is the radius of the Earth, $P_m^n(cos\theta)$ are the *Schmidt functions* (m denotes the degree of P and n the order), often used in geomagnetism, which are equivalent to Legendre polynomials. The expansion coefficients g_m^n and h_m^n are the *Gaussian coefficients*, given in units of nT, being Gauss the pioneer in spherical harmonic analysis of the Earth magnetism. [34]

The magnetic field variations are represented by the angular functions, the Schmidt functions and the Fourier series of φ, being the latitudinal and longitudinal variations respectively.

Also, the three components of the magnetic field at the Earth's surface can be obtained and expressed by the Gaussian coefficients [35]:

$$X = \frac{\partial V^{int}}{r\partial\theta} \quad Y = \frac{-\partial V^{int}}{rsin\theta\partial\varphi} \quad Z = \frac{\partial V^{int}}{\partial r}. \qquad (B.7)$$

As the geomagnetic field is properly represented by the method of spherical harmonic analysis, the approximation of no electric currents on the surface is used on the simulation, as shown in Annex A.

ANNEX C: THICKNESS INFLUENCE

The influence of the thickness on the shielding effectiveness by keeping a constant aspect or length-to-diameter ratio and using a high-μ materials flat end-cap cylinder, was studied. The S.E. was measured by choosing a specific point, which was proportionally moved as the length increased.

First, the thickness was increased while increasing the length and diameter proportionally. Starting by a cylinder with L = 140mm, D= 70mm and t= 0,14mm, the obtained results are shown in Figure 31.

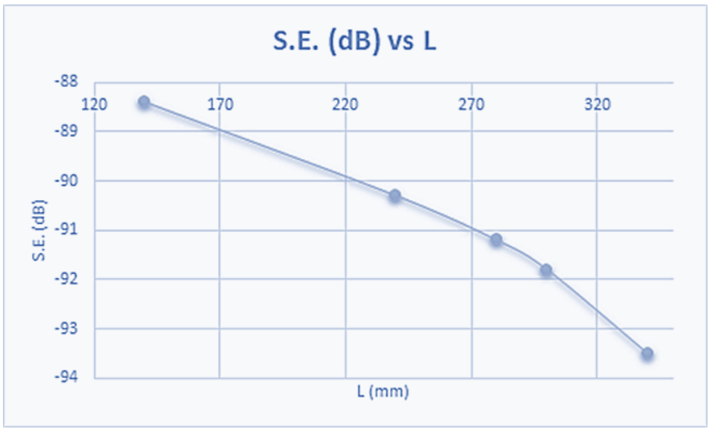

***Figure 31**. Shielding Effectiveness vs Length. Thickness and diameter were increased proportionally. Response shows enhanced shielding for L>300mm.*

Secondly, the same procedure was carried out, but the thickness was kept constant. However, as before, length and diameter were proportionally increased (Figure 32).

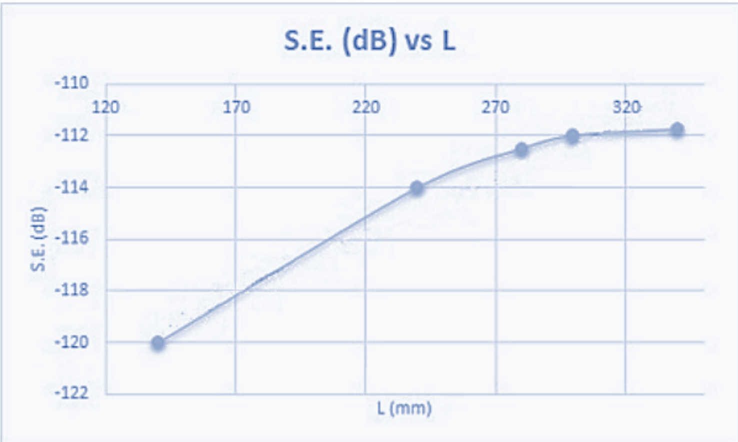

***Figure 32**. Shielding Effectiveness vs Length. Constant thickness.*

A point proportionally displaced as the length is increased is studied. As can be visualized, by increasing the thickness, the S.E. had better numbers. However, having a thicker shield, reduces the chances of having penetration on the shield.

In contrast, with a constant thickness, the opposite effect can be observed. This can be explained because of the increase of the relative distance of the chosen point regarding to the end-cap (Figure 33).

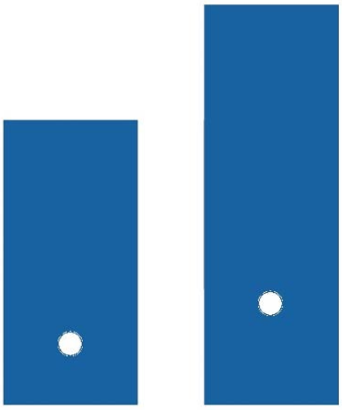

Figure 33. *Visualization of the increase of the relative distance of a chosen point regarding to the end-cap.*

The Mumetal shield had to be reduced by half in order to perform the simulation. As the thickness was proportionally reduced with the aspect ratio, a small reduction of the magnetic shielding is expected by using the original parameters.

Varying proportionally the dimensions of the studied geometry does not result in scaled results, because there is not symmetry in the studied case.